

**INVESTIGATION OF PHOTOCATALYTIC ACTIVITIES  
OF METAL OXIDE ALD THIN FILMS**

**Shafiqul ISLAM**



T.C.  
BURSA ULUDAĞ UNIVERSITY  
GRADUATE SCHOOL OF NATURAL AND APPLIED SCIENCES

**INVESTIGATION OF PHOTOCATALYTIC ACTIVITIES OF METAL OXIDE  
ALD THIN FILMS**

**Shafiqul ISLAM**  
0000-0002-3290-1386

Asst Prof. Dr. Halil İbrahim AKYILDIZ  
(Supervisor)

MSc THESIS  
DEPARTMENT OF TEXTILE ENGINEERING

BURSA – 2020  
**All Rights Reserved**



## THESIS APPROVAL

This thesis titled "INVESTIGATION OF PHOTOCATALYTIC ACTIVITIES OF METAL OXIDE ALD THIN FILMS" and prepared by Shafiqul ISLAM has been accepted as an **MSc THESIS** in Bursa Uludag University Graduate School of Natural and Applied Sciences, Department of Textile Engineering following a unanimous vote of the jury below.

**Supervisor** : Asst Prof. Dr. Halil İbrahim AKYILDIZ

**Head** : Asst Prof. Dr. Halil İbrahim AKYILDIZ  
0000-0002-8727-5829  
Bursa Uludag University,  
Faculty of Natural and Applied Science,  
Department of Textile Engineering.

Signature

**Member:** Prof. Dr. Recep EREN  
0000-0001-9389-0281  
Bursa Uludag University,  
Faculty of Natural and Applied Science,  
Department of Textile Engineering.

Signature

**Member:** Asst Prof. Dr. Ömer Yunus GÜMÜŞ  
0000-0002-3361-6528  
Bursa Technical University,  
Faculty of Engineering and Natural Sciences,  
Department of Polymer Materials Engineering.

Signature

**I approve the above result**

  
Prof. Dr. Hüseyin Aksel EREN  
Institute Director

**I declare that this thesis has been written in accordance with the following thesis writing rules of the U.U Graduate School of Natural and Applied Sciences;**

- All the information and documents in the thesis are based on academic rules,
- audio, visual and written information and results are in accordance with scientific code of ethics,
- in the case that the works of others are used, I have provided attribution in accordance with the scientific norms,
- I have included all attributed sources as references,
- I have not tampered with the data used,
- and that I do not present any part of this thesis as another thesis work at this university or any other university.

**13/01/2021**

**Shafiqul ISLAM**

## ÖZET

Yüksek Lisans Tezi

### METAL OKSİT ALD FİMLERİN FOTOKATALİTİK AKTİVİTELERİNİN İNCELENMESİ

**Shafiqul ISLAM**

Bursa Uludağ Üniversitesi  
Fen Bilimleri Enstitüsü  
Tekstil Mühendisliği Anabilim Dalı

**Danışman:** Dr. Öğr. Üyesi Halil İbrahim AKYILDIZ

Fotokatalizörler TiO<sub>2</sub> ve ZnO ince filmleri, atomik katman biriktirme ile cam kumaş üzerine biriktirildi. İnce filmlerin sonradan tavlama 450 ° C ve 600 ° C'de iki saat süreyle yapıldı. TiO<sub>2</sub> ve ZnO'nun fotokatalitik aktiviteleri, güneş simülatörü ve UV lambası altında metilen mavisi bozunma verimi kullanılarak incelenmiştir. İnce filmlerin morfolojisi FESEM ve AFM tarafından araştırıldı. ALD ince filmlerin element analizi ve kristal yapısı sırasıyla XPS ve XRD ile araştırıldı. İnce filmlerin optik özellikleri UV-Vis spektrofotometre ile incelendi. 450 °C tavlı TiO<sub>2</sub> ince film, anataz forma dönüşen ve düşük bant aralıklı enerji ile hem "biriktirildiği halde" hem de tavlama TiO<sub>2</sub> ALD ince filmlerde en yüksek fotokatalitik aktiviteyi göstermiştir. "Biriktirildiği gibi" ZnO ALD ince filmler, iyi kristalleştirilmiş altıgen wurtzit yapısı, oksijen boşluğu (Vo) ve düşük bant aralığı enerjisine sahip olmaları nedeniyle, hem TiO<sub>2</sub> hem de ZnO ALD ince filmler en yüksek fotokatalitik aktiviteler göstermiştir.

**Anahtar Kelimeler:** Fotokataliz, Atomik katman birikimi, İnce film, Fotokatalizör, Atık su arıtma. Metilen mavisi.

## **ABSTRACT**

MSc Thesis

### **INVESTIGATION OF PHOTOCATALYTIC ACTIVITIES OF METAL OXIDE ALD THIN FILMS**

**Shafiqul ISLAM**

Bursa Uludag University  
Graduate School of Natural and Applied Sciences  
Department of Textile Engineering

**Supervisor:** Asst Prof. Dr. Halil Ibrahim AKYILDIZ

TiO<sub>2</sub> and ZnO thin film photocatalysts were deposited on glass fabric by atomic layer deposition. Post annealing of the thin films was carried out at 450 °C and 600 °C for two hours. Photocatalytic activities of TiO<sub>2</sub> and ZnO were investigated by using methylene blue degradation efficiency under a solar simulator and UV lamp. The morphology of the thin films was investigated by FESEM and AFM. Elemental analysis and crystal structure of ALD thin films were explored by XPS and XRD, respectively. The optical properties of the thin films were investigated by UV-Vis spectrophotometer. 450 °C annealed TiO<sub>2</sub> thin film was exhibited the highest photocatalytic activities in both “as-deposited” and annealed TiO<sub>2</sub> ALD thin films, having transformed into anatase phase from amorphous and low bandgap energy. “As deposited” ZnO ALD thin films showed the highest photocatalytic activities compared to both TiO<sub>2</sub> and ZnO ALD thin films having well crystalized hexagonal wurtzite structure, oxygen vacancy (Vo), and low bandgap energy.

**Keywords:** Photocatalysis, Atomic layer deposition, thin films, Photocatalyst, Wastewater treatment. Methylene Blue.

## **PREFACE AND/OR ACKNOWLEDGMENT**

This thesis is based on experimental work carried out during the years 2019-2020 in the Textile Engineering department laboratory at Bursa Uludag University.

I am very grateful to Asst. Professor Halil İbrahim AKYILDIZ for his cordial guidance and support in my thesis work. I consider myself very fortunate that I have had the privilege of working under his excellent supervision.

I also would like to express my gratitude to Asst. Professor Ömer Yunus GÜMÜŞ for allowing me to use the laboratory of the Fiber and Polymer department at Bursa Technical University.

I would like to express my deepest gratitude to “Türkiye Bursları” and “Presidency for Turks Abroad and Related Communities (YTB)” for providing me a full free scholarship and support.

I would like to pay heartfelt thanks to all members of Akyildiz Research Group, specially Büşra AYDEMİR, and Sümeyye DILER, for their help throughout the period.

From the bottom of my heart, I would like to thanks my parents, brothers, and sisters, who are always encouraged and support me.

Shafiqul Islam  
13/01/2021

## CONTENTS

	<b>Page</b>
ÖZET.....	i
ABSTRACT.....	ii
PREFACE AND/OR ACKNOWLEDGMENT.....	iii
SYMBOLS and ABBREVIATIONS.....	v
FIGURES.....	vi
1. INTRODUCTION.....	1
2. THEORETICAL BASICS and LITERATURE REVIEW.....	5
2.1 Background of Photocatalysis.....	5
2.2 Mechanism of Photocatalysis.....	6
2.3 Photocatalyst Materials.....	8
2.4 Applications of Photocatalysis.....	13
2.5 Photocatalyst Thin films.....	15
2.6 Atomic Layer Deposition.....	16
2.7 Photocatalytic ALD Thin Films.....	19
3. MATERIALS and METHODS.....	21
3.1 Substrates Preparation.....	21
3.2 Thin films Growth Parameters.....	21
3.3 Annealing of ALD Thin films.....	22
3.4 Photocatalytic Activity Experiment.....	22
3.5 Characterization of ALD Thin films.....	24
3.5.1. Field Emission Scanning Electron Microscope (FESEM).....	24
3.5.2 Atomic Force Microscope (AFM).....	25
3.5.6 UV-Vis Spectrophotometer.....	25
3.5.7 X-ray Diffractometer Analysis (XRD).....	28
3.5.8 X-ray photoelectron spectroscopy (XPS).....	28
4. RESULTS and DISCUSSION.....	29
4.1 FESEM Image of ALD TiO <sub>2</sub> and ZnO Thin Films.....	29
4.2 AFM Analysis of ALD Thin Films.....	31
4.3 XPS Analysis of ALD Thin Films.....	32
4.4 XRD Pattern of ALD Thin Films.....	40
4.5 UV-Vis Absorbance Spectra and Bandgap Analysis.....	42
4.6 Photocatalytic Activity Test of ALD Thin Films.....	45
5. CONCLUSION.....	52
REFERENCES.....	53
RESUME.....	67

## SYMBOLS and ABBREVIATIONS

<b>Symbols</b>	<b>Definition</b>
$\alpha$	Absorbance Co-efficient
$\nu$	Frequency
$h$	Plank Constant
$E_g$	Photon Energy
$\lambda$	Wavelength
$I$	Incident Light
$I_o$	Transmitted Light

<b>Abbreviation</b>	<b>Definition</b>
ALD	Atomic Layer Deposition
MB	Methylene Blue
FESEM	Field Emission Scanning Electron Microscope
AFM	Atomic Force Microscope
XPS	X-ray Photoelectron Spectroscopy
XRD	X-ray Diffractometer
UV-Vis	UV-Vis Spectrophotometer
TDMAT	Tetrakis (Dimethylamido) Titanium
DEZ	Diethylezinc
RMS	Root Means Square
AOP	Advance Oxidation Process
BE	Binding Energy
TFD	Thin Film Deposition

## FIGURES

	<b>Page</b>
Figure 1: The degradation mechanism of organic pollutants via photocatalysis (Samsudin et al. 2015).....	7
Figure 2: Generation of active oxygen species resulting in solar irradiation of TiO <sub>2</sub> (Hoffmann et al. 1995).....	7
Figure 3: Thin-film growing mechanism of the atomic layer deposition technique (Johnson et al. 2014). ....	18
Figure 4: Experiment Flow Chart. ....	21
Figure 5: Savannah ALD system. ....	22
Figure 6: Photocatalytic Experiments Under (a) & (b) Solar Simulator and (c) & (d) Under UV Lamp.....	24
Figure 7: Beer-Lambart law of Absorption.....	27
Figure 8: FESEM Image of “as deposited”TiO <sub>2</sub> (a) and ZnO (b); 450 °C Annealed TiO <sub>2</sub> (c) and ZnO (d); 600 °C Annealed TiO <sub>2</sub> (e) and ZnO (f) ALD thin films & Pristine Glass Fabric (g).....	30
Figure 9: AFM Image of “as deposited”TiO <sub>2</sub> (a) and ZnO (b); 450 °C Annealed TiO <sub>2</sub> (c) and ZnO (d); 600 °C Annealed TiO <sub>2</sub> (e) and ZnO (f) ALD thin films.....	32
Figure 10: XPS Survey Spectra of TiO <sub>2</sub> (a) and ZnO ALD Thin film. ....	34
Figure 11: High-resolution C 1s XPS spectra of “as deposited”TiO <sub>2</sub> (a) and ZnO (b), 450 °C annealed TiO <sub>2</sub> (c) and ZnO (d), 600 °C annealed TiO <sub>2</sub> (e) and ZnO (f) ALD thin films. ....	36
Figure 12: High-resolution O 1s XPS spectra of “as deposited”TiO <sub>2</sub> (a) and ZnO (b), 450 °C annealed TiO <sub>2</sub> (c) and ZnO (d), 600 °C annealed TiO <sub>2</sub> (e) and ZnO (f) ALD thin films. ....	38
Figure 13: High-resolution 2p XPS spectra of “as deposited”TiO <sub>2</sub> (a) and ZnO (b), 450 °C annealed TiO <sub>2</sub> (c) and ZnO (d), 600 °C annealed TiO <sub>2</sub> (e) and ZnO (f) ALD thin films. ....	40
Figure 14: XRD pattern of TiO <sub>2</sub> (a) and ZnO ALD thin films.....	42
Figure 15: UV-Vis Absorption spectra of TiO <sub>2</sub> (a) and ZnO (b) ALD thin films. ....	43
Figure 16: Tauc plot of TiO <sub>2</sub> (a) and ZnO (b) ALD thin films.....	44
Figure 17: Photocatalytic Activities of TiO <sub>2</sub> (a) and ZnO (b) ALD Thin Films Under Dark Medium. ....	46
Figure 18: Photocatalytic Activities Test of TiO <sub>2</sub> (a) and ZnO (b) ALD thin films under Solar Simulator. ....	49
Figure 19: Photocatalytic Activities Test of TiO <sub>2</sub> (a) and ZnO (b) ALD thin films under UV lamp. ....	51



## 1. INTRODUCTION

Air, water, and soil are the essential environmental elements of nature being polluted enormously every day. Freshwater is being contaminated by different industries and agricultural activities that may cause temporary or permanent damage to the life of all species (Schwarzenbach et al. 2010). The polluted water accommodates hazardous wastes like textile dyes, pesticides, herbicides, pharmaceutical wastes, resins, and phenolic compounds (Chong et al. 2010, Konstantinou ve Albanis 2004, L. Zhang ve Fang 2010). The textile and industrial dyeing processes are the key accountable for producing organic pollutants that spontaneously contaminate freshwater sources. About 1-20% of the total world production of dyes is released to the freshwater source during the different textile manufacturing processes (Akpan ve Hameed 2009, Konstantinou ve Albanis 2004). Moreover, the textile industries consume the highest amount of freshwater for the different steps of textile processing, and discharged waters are also highly polluted. The average size of a textile factory requires approximately 200 L of water to process one kg of fabrics per day and release a vast amount of wastewater to the freshwater sources (Holkar et al. 2016, Yaseen ve Scholz 2019).

Textile wastewater can be treated with physical, biological, oxidation methods or a combination of them (Holkar et al. 2016). Physical treatment methods like coagulation/flocculation, adsorption, and filtration are not completely removed the toxic materials from the wastewater. Moreover, coagulation/flocculation treatment methods do not show the same decolorization efficiency for various dye-containing wastewater, and it produces a large amount of sludge. This sludge need to disintegrate as a subsequent step, causing the process cost increases (Liang et al. 2014, Yeap et al. 2014). Adsorption shows better decolorization efficiency for various dye-containing wastewater using an adsorbent like activated carbon. However, adsorbents are highly expensive and produce a lot of sludge as well (Gupta et al. 2011). Filtration techniques like ultrafiltration (UF), nanofiltration (NF), and reverse osmosis (RO) are another group of techniques that are used to treat textile wastewater. It can reduce the biological oxygen demand (BOD), chemical oxygen demand (COD), and color of textile wastewater simultaneously (Chollom et al. 2015). However, the initial investment of the treatment method is expensive, and it generates other waste, including water-insoluble dye (e.g., indigo dye),

that requires another treatment to remove (Hoek et al. 2013). The biological treatment methods have been used to remove toxic materials from textile wastewater. On the basis of using oxygen, the biological treatment can be classified into two major groups, and they are aerobic and anaerobic (Holkar et al. 2016). Due to the recalcitrant nature of the synthetic dye and the high salinity of wastewater, biological treatment methods less effective in removing toxic materials from the textile wastewater (Khan et al. 2017) and also produce sludge (Holkar et al. 2016). Chemical wastewater treatments are considered the most effective wastewater treatment methods compared to other treatment methods. Chemical wastewater treatments can be classified into the chemical oxidation process and advance oxidation process (AOP). In chemical oxidation methods, oxidants like  $O_3$ ,  $H_2O_2$  have been used to treat textile wastewater. Ozone and  $H_2O_2$  form strong non-selective hydroxyl radicals at high pH, and this hydroxyl radical considers the most powerful oxidant having 2.33 oxidation potential, which can oxidize the majority of the organic pollutants present in textile wastewater (Tehrani-Bagha et al. 2010). The chemical oxidation process may have less effective in comparison to advanced oxidation processes (AOP) such as Fenton reagent and photocatalysis, due to it produces less amount of hydroxyl radicals in comparison to the advance oxidation process (AOP). Fenton reagent is a very effective AOP method that can degrade the soluble and insoluble dye in textile wastewater, but the disadvantage of this method is iron sludge production (Babuponnusami ve Muthukumar 2014). Photocatalysis is projected to be one of the best AOP methods for removing organic waste substances from textile wastewater. It can decompose the organic pollutant entirely with the help of solar energy and photocatalyst without producing chemical sludge (Fujishima et al. 2000, Rajeshwar et al. 2008, Rehman et al. 2009). Photocatalysis is an economical wastewater treatment method because it uses solar energy available in the environment and the availability of photocatalyst. Moreover, it requires a mild atmospheric condition such as a mild temperature and pressure. Two types of photocatalysts, homogenous and heterogeneous catalyst, have been used in photocatalysis methods. Heterogeneous catalysts such as  $TiO_2$ ,  $ZnO$ ,  $SnO$ , and  $CeO_2$  show better photocatalytic activity than homogenous catalyst because of their unique electronic structure, that is, the electron fill valance band and empty conduction band (Fujishima et al. 2000, Khan et al. 2015, Konstantinou ve Albanis 2004, Nakata ve Fujishima 2012, Rehman et al. 2009). During a photocatalytic process, as the photons

reach the surface of a photocatalyst, the electrons of a catalyst are getting excited via the absorption of the photon energy. When the electrons absorb enough energy (i.e., equal to their band gap or higher), they are promoted to the conduction band by leaving positively charged holes in the valence band. These holes react with water molecules which is available to the surface of the catalysts and generate hydroxyl radicals ( $\cdot\text{OH}$ ) that have the strong oxidizing power resulting in the complete degradation of organic pollutant into  $\text{H}_2\text{O}$ ,  $\text{CO}_2$  and non-toxic substances (Fujishima et al. 2000, Khan et al. 2015, Rajeshwar et al. 2008, Rehman et al. 2009).

There are various thin film methods have been introduced to fabricate photocatalyst thin films on a substrate such as sol-gel (Garzella et al. 2000, Yu et al. 2001), sputtering methods (Miao et al. 2003, Takeda et al. 2001), pulse laser deposition (PLD) (Suda et al. 2005), spray pyrolysis (Suda et al. 2005), physical vapor deposition (PVD) (Rosnagel 2003), chemical vapor deposition (CVD) (Byun et al. 2000), and atomic layer deposition (ALD). Atomic layer deposition is a vapor phase deposition technique that is a modified version of CVD, and it is considered the most convenient method to deposit nanostructured thin films on a substrate because of its sequential and self-limiting surface reactions. During the ALD process, a substrate is exposed to a precursor that reacts only with the surface of the substrate until saturating the surface with a monolayer. The unreacted species and by-products from the surface reaction are removed subsequently by the purging of an inert gas such as Ar or  $\text{N}_2$ . After that, a second precursor is exposed to the surface and reacts with the previous monolayer forming a layer of desired thin-film material on the substrate. This one exposure-purge-one exposure-purge sequence is called one ALD cycle. Since there is no chance to occur other gas-phase reactions, the desired thin film is grown layer by layer on the substrate so that the thickness of the thin film can be precisely controlled by counting the repeated cycle. It also gives conformal, uniform, and can deposit ultra-thin approximate angstrom ( $10^{-10}$  m) level of thickness. The other advantage of ALD, it can deposit thin film at vacuum and low temperature so that the temperature-sensitive materials such as polymers can be coated by ALD (Dasgupta et al. 2015, Guo et al. 2017, G. K. Hyde et al. 2009, G. Kevin Hyde et al. 2007, Iqbal et al. 2016, Johnson et al. 2014, Jur et al. 2011, Van Bui et al. 2017). In addition, ALD can create films of different groups of materials such as metals (H. Kim 2003), metal

oxides (Potts et al. 2010), metal nitrides (J. Kim et al. 2003), metal sulfides (Dasgupta et al. 2015), and many others.

In this study, photocatalytic activities of ALD TiO<sub>2</sub> and ZnO metal oxides have been investigated under the solar simulator and UV lamp separately. ALD thin films have been deposited on the fibrous structure of glass fabrics to use the highest surface area of the substrate to explore the photocatalytic activities of the thin films. The effect of different annealing temperatures to observe the change of grain size, morphological structure, and variation of photocatalytic activities of the thin films also have been investigated.

## 2. THEORETICAL BASICS and LITERATURE REVIEW

In this part, the background of photocatalysis, mechanism of photocatalysis, different type of photocatalyst metal oxide, application of photocatalyst, a different type of thin-film deposition methods, the principle of ALD thin film formation, and photocatalyst ALD have been discussed.

### 2.1 Background of Photocatalysis

Photocatalysis is a promising environment-friendly technique for removing pollutants from water, air, and soil. In this technique, solar energy can be used for the elimination of toxic contaminants with the help of photocatalytic materials. Photocatalysis has been getting immense attention from researchers from around the world. More than 16000 articles have been published in the last ten years regarding photocatalysis, and every year the number of publications has been increasing as well (Rueda-Marquez et al. 2020).

Before the discovery of photocatalysis, the semiconductor metal oxide materials such as  $\text{TiO}_2$  was used as a white pigment since ancient times because they were chemically stable, cheap, and innocuous. The activity  $\text{TiO}_2$  remained inactive in a dark medium, but it showed a chemical reaction under UV light (Serpone et al. 2012). The studies on the photoactivity of  $\text{TiO}_2$  have been started in the early part of the 20<sup>th</sup> century. In 1938 a report published on the photo-bleaching by  $\text{TiO}_2$  both in vacuum and in an oxygen environment, under irradiation of UV light, producing active oxygen that caused the photo-bleaching of dye species. On that report, "Photosensitizer"  $\text{TiO}_2$  had been used instead of the terminology "Photocatalyst" (Goodeve ve Kitchener 1938). In 1956, Mashio *et al.* demonstrated that the oxidation of organic compounds such as alcohol, hydrocarbon, and production of  $\text{H}_2\text{O}_2$  after dispersing  $\text{TiO}_2$  powder into an organic solution under the UV illumination (Hashimoto et al. 2005). Later in 1969, Fujishima and Honda, used a single crystal n-type  $\text{TiO}_2$  (rutile) as a semiconductor electrode to investigate the photo-electrolysis of water. When the  $\text{TiO}_2$  electrode was exposed to the UV light, the current had been generated from the counter platinum electrode to the  $\text{TiO}_2$  electrode. They reported that the photolysis of water could be achieved by using  $\text{TiO}_2$  electrodes, only exposed to UV light, and no usage of external voltage in the system (Fujishima, A., and Honda 1972). In 1980 when the energy crisis had surged, many

researchers gave their attention to produce H<sub>2</sub> gas by using photocatalysis (Kawai ve Sakata 1980), but TiO<sub>2</sub> photocatalyst can only absorb UV light irradiation that is just 4% of the total solar spectrum. For this reason, H<sub>2</sub> production in this method was made researchers less interested in that time. Later, as the oxidizing power of TiO<sub>2</sub> was discovered, the research interest shifted to decompose the harmful contaminant from water by using TiO<sub>2</sub> as a photocatalyst (Frank ve Bard 1977, Matthews 1987). Currently a significant number of research articles have been published on wastewater treatment and other areas by photocatalysis every year.

## **2.2 Mechanism of Photocatalysis**

Photocatalysis is one kind of photochemical reaction assists by the photocatalyst materials and light energy. When photons irradiate the surface of photocatalyst material, a series of redox reactions occur on the surface of the photocatalyst. Semiconductor photocatalysts have a unique electronic structure characterized by an electron filled valance band and an empty conduction band. When solar energy falls on the surface of a photocatalyst, the electrons of the valance band get excited. If the electrons get enough energy equal to or more than the bandgap energy, the electrons are promoted to the conduction band, leaving holes (h<sup>+</sup>) on the valance band. The h<sup>+</sup> (hole) is considered the strong oxidizing agent is having redox potential ranging from +1.0 to +3.5 V (measured vs normal hydrogen electrode, NHE at room temperature) relying on the type of semiconductor and pH (Hoffmann et al. 1995). This (h<sup>+</sup>) strong oxidizing agent can directly decompose the organic pollutant or can be reacted with water, generating powerful oxidizing agent hydroxyl radical (•OH) containing redox potentials 2.8 V that decompose the organic pollutants into CO<sub>2</sub>, H<sub>2</sub>O, and non-toxic substances. Fig.1 represents the total photocatalysis mechanism to degrade the organic pollutant into CO<sub>2</sub>, H<sub>2</sub>O, and non-toxic substance.

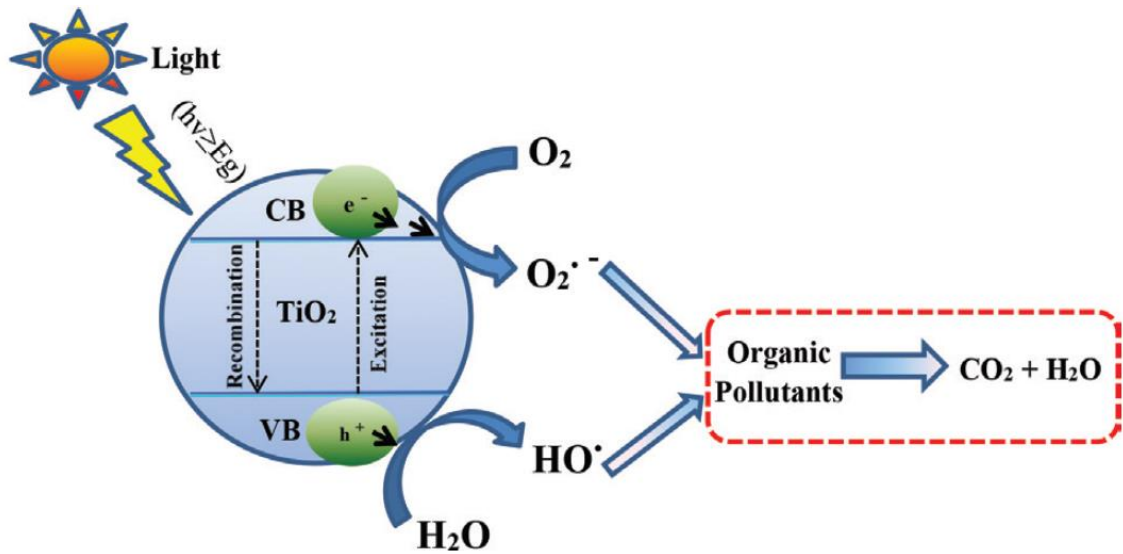


**Figure 1:** The degradation mechanism of organic pollutants via photocatalysis (Samsudin et al. 2015).

Fig. 2 shows the possible generation of activated oxide species during the photocatalysis.

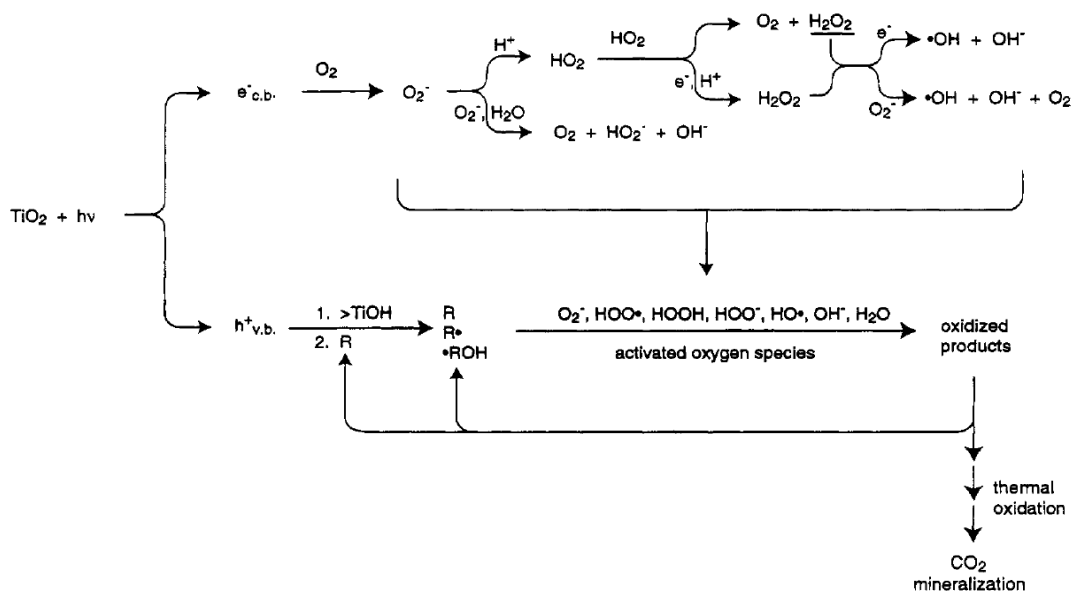


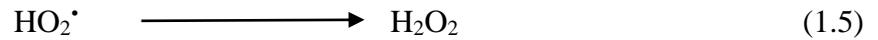
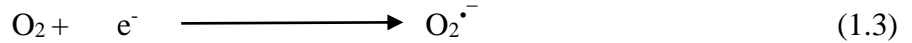
**Figure 2:** Generation of active oxygen species resulting in solar irradiation of TiO<sub>2</sub> (Hoffmann et al. 1995).

Equation (1.1) and (1.2) represent the oxidation reaction between h<sup>+</sup> (hole) and H<sub>2</sub>O to generate the hydroxyl radical (J. Zhang et al. 2018).





The electrons promoted to conduction band via photoexcitation need to eliminate from it to avoid the recombination with the hole ( $h^+$ ) present in the valance band to enhance the photocatalytic activity. As the aim of this photoreaction is to decompose the organic pollutants, oxygen can be employed as a scavenger that may be available on the surface of the photocatalyst. The reduction of the oxygen may produce the following species shown in the equation (1.3) to (1.8) (J. Zhang et al. 2018).



Both oxidation and reduction reaction produces hydroxyl radical, which is considered the most strong oxidant. The hydroxyl radical reacts with the organic pollutant and decompose them into  $CO_2$ ,  $H_2O$ , and non-toxic materials (Hoffmann et al. 1995, Rajeshwar et al. 2008, Samsudin et al. 2015). As the hole ( $h^+$ ) reacts with water and the electron ( $e^-$ ) reacts with the oxygen during photocatalysis, the production of electrons-holes generation have been accelerated; as a result, the photodegradation of organic pollutant is increased.

### 2.3 Photocatalyst Materials

There are two types of photocatalysts that have been used in the photocatalysis technique. They are homogenous and heterogeneous photocatalysts. In literature, it has been reported that heterogeneous photocatalysis has better photocatalytic activity than homogenous photocatalyst (S. Kim et al. 2004). Semiconductor metal oxides are considered the heterogeneous photocatalyst contained a unique electronic structure characterized by electron full valance band and empty conduction band. Semiconductors such as  $TiO_2$ ,  $ZnO$ ,  $Fe_2O_3$ ,  $CdS$ ,  $CeO_2$ ,  $SnO$ ,  $Al_2O_3$  and their doped are used as a photocatalyst. Photocatalytic activity of semiconductor greatly depends on the electrical structure, energy bandgap between valance band and conduction band, visible and UV

light absorption ability, the electron-hole recombination, and charge carrier phenomena. These features are considered for choosing a photocatalyst.

TiO<sub>2</sub> is the most widely used semiconductor photocatalyst due to its chemical stability, non-toxic in nature, biocompatibility, physical, optical and electronic properties. It has a high melting point of 1855 °C and is insoluble in various solutions, including water, HNO<sub>3</sub>, HCl, and dilute H<sub>2</sub>SO<sub>4</sub>. On the contrary, hot H<sub>2</sub>SO<sub>4</sub> and HF can dissolve TiO<sub>2</sub> (J. Zhang et al. 2018). The chemical structure and electronic structure of TiO<sub>2</sub> is highly commensurate for photocatalytic activity. The valance band is densely filled with the electrons, while the conduction band is empty. This electronic structure makes the TiO<sub>2</sub> one of the most effective photocatalysts, among others. It is reported that the crystal structure of TiO<sub>2</sub> greatly influences the photocatalytic activity of it. The primary crystal structure has been found for TiO<sub>2</sub> are anatase, rutile, and brookite. The anatase crystal structure shows higher photocatalytic activities than rutile and brookite (Fang et al. 2011). The bandgap of anatase and rutile differ from each other, which also influences their photocatalytic activity. The bandgap of anatase TiO<sub>2</sub> is 3.2 eV, while the rutile is 3.0 eV (Kavan et al. 1996). As the large bandgap of anatase TiO<sub>2</sub>, it needs a small wavelength of light ( $\lambda < 388$  nm) to generate electron-hole that is considered the major drawback of TiO<sub>2</sub>. There are many techniques that have been employed to enhance the photocatalytic activities of TiO<sub>2</sub> under visible light and UV light. As the electronic conductivity of anatase TiO<sub>2</sub> can be increased by creating oxygen defect or adding impurity to it. Thus the photocatalytic activity of anatase TiO<sub>2</sub> can be influenced by creating deficient oxygen and adding impurity (Liu et al. 2009). Other methods, such as doping, adding noble metals (e.g., Au, Ag), or nanocomposite of TiO<sub>2</sub> may increase the photocatalytic activities of TiO<sub>2</sub> under UV light and visible light. The nanostructure of TiO<sub>2</sub> has shown the highest photocatalytic due to its high surface area, and it is known that containing a high surface area of a catalyst has shown higher photocatalytic activities than a low surface area. It is also reported that various nanostructures of TiO<sub>2</sub>, such as a nanoparticle, nanotube, and ultra-thin film, have shown different photocatalytic activities. For instance, the nanotube of TiO<sub>2</sub> has shown better antibacterial activity than the immobile nanoparticles and ultra-thin film (Molina-Reyes et al. 2020). Therefore it is important to choose the specific nanostructure of TiO<sub>2</sub> for the specific application. The TiO<sub>2</sub> photocatalyst has been

employed in various research fields. It has been used for environmental applications such as purifying water, air, and soil, to produce self-cleaning surface, antibacterial activity, to produce wettable surface, anti-fogging function (Hashimoto et al. 2005). It is also employed for energy production such as H<sub>2</sub> (Ni et al. 2007) and hydrocarbons (Razzaq et al. 2017) by using a photoreduction mechanism.

ZnO semiconductor has been employed as photocatalyst as well because it contains similar characteristics as TiO<sub>2</sub>. As an alternative photocatalyst to TiO<sub>2</sub>, ZnO provides similar bandgap energies but exhibits higher absorption efficiency compared to TiO<sub>2</sub> over the solar spectrum (Qiu et al. 2008). Fenoll et al. reported that the photodegradation of fungicides in leaching water using ZnO and TiO<sub>2</sub> under solar irradiation was compared and found that ZnO exhibited better photodegradation activities under solar irradiation in comparison to TiO<sub>2</sub> (Fenoll et al. 2011). ZnO has excellent electrical, mechanical, and optical characteristics similar to TiO<sub>2</sub> (Gharoy Ahangar et al. 2015). ZnO can be found in three crystal forms such as hexagonal wurtzite, cubic zinc-blende, and rocksalt (Espitia et al. 2012). It contains inherent defects such as oxygen vacancy (VO), Zn interstitial (Zn<sub>i</sub>), and zinc vacancies (VZn), influencing its optical properties and electrical behavior (Boukos et al. 2012). As mentioned before, the surface area of photocatalysts has been played an important role in photocatalytic activities. The nanostructures of ZnO have been employed for photocatalysis. The nanostructure such as nanoparticles, nanorod, nanofiber, nanowire, nanotube, a nanoplate, and thin-film have higher surface areas than bulk structures, but among the nanostructure, the surface area may vary and photocatalytic activities as well. For instance, ZnO nanoplate showed higher photocatalytic activities than ZnO nanorod for having a higher surface area (Jang et al. 2006). The main limitation of ZnO has high recombination of electron-hole pairs and low charge carrier possibility. Different methods have been employed to increase the photocatalytic activities of photocatalysts, such as metal/non-metal doping, coupling with other semiconductors, and the coupling of nanocarbon with ZnO (Ong et al. 2018). Due to the presence of Zn – O – Zn bonds in ZnO nanostructure, agglomeration may happen readily and thus significantly affect the photocatalytic activity. To avoid the agglomeration of ZnO nanoparticles, surface modification has been utilized through chemical treatments such as coating, grafting polymerization, and ligand exchange (Ong

et al. 2018). As a photocatalyst, ZnO semiconductor gets immense interest after TiO<sub>2</sub> semiconductor.

Fe<sub>2</sub>O<sub>3</sub> semiconductor has also been employed as a photocatalyst itself or doped with other semiconductors such as Ti, Zn, and other metals. A different form of crystal structure has been found for Iron oxides such as wüstite (FeO), hematite ( $\alpha$ -Fe<sub>2</sub>O<sub>3</sub>), maghemite ( $\gamma$ -Fe<sub>2</sub>O<sub>3</sub>), and magnetite (Fe<sub>3</sub>O<sub>4</sub>). Among them, hematite ( $\alpha$ -Fe<sub>2</sub>O<sub>3</sub>) has been exerted for photocatalytic activities because of its suitable crystal and chemical structure, stability at ambient conditions, and having a low bandgap ( $E = 2.1$  eV) (L. X. Chen et al. 2002). Due to its small bandgap of about 2.0–2.2 eV, Hematite (or  $\alpha$ -Fe<sub>2</sub>O<sub>3</sub>) is a promising photocatalytic candidate. In addition, it can absorb solar energy up to 600 nm and utilizes up to 40 percent of solar spectrum energy, and can remain stable in most aqueous solutions (pH>3). However, the photocatalytic efficiency of  $\alpha$ -Fe<sub>2</sub>O<sub>3</sub> is restricted by certain factors such as a high electron and hole recombination, poor diffusion, short hole diffusion length (2-4 nm), and poor conductivity, that lowering the photocatalytic activities of it (Sartoretti et al. 2003)(Ahn et al. 2014). Researchers have made several efforts to solve those problems, including minimizing the recombination rate by forming nanostructures, improving conductivity by doping with appropriate metals, and improving charge carrying ability as well (Kumari et al. 2007, Zandi et al. 2013).

CdS is considered one of the most prominent semiconductor photocatalysts for photocatalytic activities among various sulfides, is a visible light-reactive photocatalyst with a bandgap of 2.4 eV, and it has good efficiency at a wavelength shorter than 516 nm for visible light absorption. Furthermore, it has an excellent charge carrying power, which can easily and effectively render photogenerated electrons and holes moving, prolong the photogenerated carrier's life, and contribute to high photocatalytic action (F. Chen et al. 2008). The main drawback of CdS is photo-corrosion. Intense research has been conducted to inhibit the photo-corrosion of CdS by employing various processes such as CdS integration into other layers of oxides, CdS combination with microporous and mesoporous materials, metal and non-metallic catalyst coupling, and heterojunction forming nanoparticles (Cheng et al. 2018). As a photocatalyst, CdS semiconductors mainly used energy production and environmental application (Cheng et al. 2018).

CeO<sub>2</sub> semiconductor has been considered as excellent photocatalyst because of its high oxygen storage ability with abundant oxygen vacancies (Vo), Ce<sup>3+</sup>/Ce<sup>4+</sup> due to reversible pairs and its inhibition to photo-corrosion (Gong et al. 2016). The main drawback of this photocatalyst is the wide-bandgap energy, which is 2.8-3.1 eV and can only absorb the UV region and partially in the visible region up to 400 nm, which is less than 5% of the solar spectrum (Aslam et al. 2016). Therefore to enhance the photocatalytic activities of CeO<sub>2</sub> under visible light, various methods have been employed on it, such as metal or non-metal doping, doped with noble metal (Au, Ag), coupling with other nanomaterials. It is reported that after modification with one of these, photocatalytic activities had been significantly increased under visible light (Ma et al. 2019).

SnO<sub>2</sub> semiconductor is considered an alternative photocatalyst for TiO<sub>2</sub> due to being low cost and innocuous photocatalyst analogous to TiO<sub>2</sub> (Al-Hamdi et al. 2017). In addition, its unique chemical structure, containing the octahedral network in its structure, makes it more favorable for photocatalytic activities because of enhancing the mobility of electron-hole pairs (Abe et al. 2006). Furthermore, SnO<sub>2</sub> has an intrinsic defect (oxygen vacancy) on its crystal structure, resulting in the reduction of the bandgap, which may lead to an increase in the photocatalytic activities of it (Zulfiqar et al. 2016). However, the main disadvantage of SnO<sub>2</sub> is high bandgap energy, which is 3.6 eV, require to absorb only UV light to generate electron-holes, and also has a high electron-hole recombination rate (Al-Hamdi et al. 2017). Therefore, to inhibit the recombination rate and enhance the photocatalytic activity, various methods have been employed on SnO<sub>2</sub> as like other semiconductors. For instance, coupled with other semiconductors, doped with metal and metalloids, transition metal and non-metal are mostly used techniques for improving the photocatalytic activity of SnO<sub>2</sub> semiconductor (Al-Hamdi et al. 2017). However, different nanostructure and different synthesis methods may have an impact on the photocatalytic activities of SnO<sub>2</sub>. For instance, SnO<sub>2</sub> quantum dots has been prepared by Bhattacharjee & Ahmaruzzaman, showing significant photocatalytic activities to degrade the Methylene blue (MB) and Rose Bengal under sunlight irradiation (Bhattacharjee ve Ahmaruzzaman 2015).

Al<sub>2</sub>O<sub>3</sub>, itself does not exhibit photocatalytic activities due to its high energy bandgap, which is 8.7 eV (Leow et al. 2017). However, it has been shown photocatalytic activities

even under visible light when it is doped or coupled with other semiconductors. For instance, Barajas et al. reported that Al<sub>2</sub>O<sub>3</sub> doped with rutile TiO<sub>2</sub> thin film exhibit visual light-induced photocatalytic activities to kill the *E. coli* bacteria (Barajas-Ledesma et al. 2010). Nasr et al. prepared Al<sub>2</sub>O<sub>3</sub> doped ZnO nanotube by ALD, demonstrated Al<sub>2</sub>O<sub>3</sub> doped ZnO nanotube exhibited five times higher photocatalytic activities than ZnO nanotube to decompose the methylene orange (Nasr et al. 2018).

Photocatalytic activities of semiconductor metal oxides are greatly dependent on their chemical and crystal structure, surface area, charge-carrying ability, electron-hole recombination possibility, and UV light and visible absorption ability. In literature, it is reported that the photocatalytic activity of semiconductors can be increased significantly by doping each other, metal, noble metal (Ag, Au), or non-metal (C, N, S). Researches are still ongoing to produce visible light effective and economical photocatalyst for energy production (H<sub>2</sub>, Fuel) and environmental remediation.

#### **2.4 Applications of Photocatalysis**

In this part, we will discuss the wide range of applications of photocatalysis in different areas. As mentioned above, photocatalysis has been used to clean the wastewater. Apart from this, the photocatalysis method has been employed in preparing self-cleaning surfaces, antimicrobial activities, and energy harvesting phenomena.

The photocatalysts have been used for producing a self-cleaning surface due to their hydrophilic nature when exposed to UV or visible light. In 1997, Wang et al. reported the photo-induced super hydrophilic effect of TiO<sub>2</sub>, and since then, the phenomenon has been under intense study (Rong Wang et al. 1997). It was shown that the TiO<sub>2</sub> surface becomes extremely hydrophilic after irradiation under UV light. The commercial self-cleaning surface has been produced by using TiO<sub>2</sub> thin films. For instance, the self-cleaning windows have been developed by Pilkington, PPG, and Saint Gobain. The surface photocatalytic reactions of TiO<sub>2</sub> break up the organic stain, thus cleaning the surface when UV light is irradiated. Wang et al. attributed that water flow (such as rainwater) to the stain contained TiO<sub>2</sub> surface made TiO<sub>2</sub> super hydrophilic that enhanced the self-cleaning performance of TiO<sub>2</sub> surface (Rang Wang et al. 1998)(Fujishima et al. 2008). Apart from the window, to avoid fouling on a different surface, such as bathtub

tiles, lamp coverings in a highway tunnel, walls, etc., photocatalytic self-cleaning surfaces have been used. This phenomenon is also used to produce anti-fogging surfaces such as bathroom tiles and car mirrors (Fujishima et al. 2008). Self-cleaning cotton fabrics and PET fabrics have also been developed by coating with nanostructures of TiO<sub>2</sub> via different methods (Jinfeng Wang et al. 2015).

The antimicrobial surfaces can be produced by fabricating nano-structure photocatalyst due to its photocatalytic activities under light energy. The reactive oxygen species have been produced from the photocatalyst during the photocatalytic reaction, have the ability to degrade the cell wall of microbes, and to oxidize them into H<sub>2</sub>O, CO<sub>2</sub>, and mineral acids (Qi et al. 2017, Yadav et al. 2016). Photocatalysis has proved capable of destroying a wide range of species, including Gram-negative and Gram-positive bacteria, including endospores, fungi, algae protozoa, and viruses (Matsunaga et al. 1988, Wolfrum et al. 2002). The photocatalytic activities of materials on antimicrobials species have been improved by modifying photocatalyst nanostructure with metal, non-metal, noble metal, heterojunction construction, and coupling with carbon materials (Qi et al. 2017, Yadav et al. 2016). Wong et al. reported that Nitrogen-doped TiO<sub>2</sub> exhibited better visible-light-induced photocatalytic activities than pure TiO<sub>2</sub> and Carbon-doped TiO<sub>2</sub> in response to *E.coli* bacteria (Wong et al. 2006). Kangwansupamonkon et al. investigated the antimicrobial effects of cotton fabrics coated with apatite TiO<sub>2</sub>. The antibacterial activities were observed under black light (wavelength 300–400 nm), visible light (wavelength 400–650 nm), and dark conditions. Under the black-light treatment, apatite-coated TiO<sub>2</sub> suspensions showed better antimicrobial activity against four different bacteria (*Staphylococcus aureus*, *Escherichia coli*, *methicillin-resistant Staphylococcus aureus (MRSA)*, and *Micrococcus luteus*) than visible light and dark conditions (Kangwansupamonkon ve Lauruengtana 2009).

Photocatalysis technology also has been applied to produce renewable and sustainable energy fuels by using solar energy. Recently, a wide range of research has been carried out on it due to the amount of fossil energy in all world is decreasing day by day. On that point, photocatalysis is a promising technique to produce energy with the help of solar energy. Moreover, photocatalysis is an environmentally friendly technique, and it can reduce the amount of CO<sub>2</sub> by photoreduction while producing energy. Hydrogen gas and

fuel like methane, ethane have been generated by the photocatalysis method. Unlike other photocatalytic activities such as wastewater treatment or antimicrobial activities, photoreduction phenomena have been employed to generate energy. The H<sub>2</sub> gas has been produced by the photocatalytic water splitting technique. When light irradiated on the photocatalyst surface, an electron-hole has been generated. Then electron-hole are diffused to the photocatalyst surface containing water molecule in it. A redox reaction occurs, in which the photoelectrons reduce the H<sup>+</sup> into H<sub>2</sub> gas, and the holes (h<sup>+</sup>) oxidize the water into O<sub>2</sub> (Singh ve Dutta 2018). For hydrocarbon fuel production, the photoreduction of CO<sub>2</sub> has been done with H<sub>2</sub>O on the surface of photocatalysts (Vu et al. 2019). A wide range of semiconductor metal sulfides (CdS) and oxides (TiO<sub>2</sub>, ZnO, CdS, SnO<sub>2</sub> and WO<sub>3</sub>) have been employed as a photocatalyst to produce the energy with all having some limitations such as wide-bandgap. As a consequence, they only absorb UV light, which is only 4% of the solar spectrum, and end up with high electron-hole recombination rates (Singh ve Dutta 2018). Several methods have been employed to modify the surface of photocatalysts such as metal (Nb, Ce, Mn, Zn, Mg, Sn, Cu, and Zr) /non-metal (B, N, F, Ca, S) doping, noble metal (Ag, Au, Pt) doping, dye sensitization (safranine, O/EDTA, and T/EDTA) and integration with metal-organic frameworks (MOF) (Singh ve Dutta 2018, Vu et al. 2019) to utilize the visible light of solar spectrum. Production of visible light-activated, stable, and economical photocatalysts for energy harvesting is still researched.

## **2.5 Photocatalyst Thin films**

In the conventional photocatalysis process, photocatalyst powder (i.e., TiO<sub>2</sub>) is used to degrade the organic pollutant for wastewater treatment. But, using the powder form of photocatalysts for wastewater treatment may have some drawbacks that greatly influences the whole photocatalytic process. The powder photocatalyst has a poor settle ability, and it takes a long retention time in the clarifier. In addition, the high turbidity generated by the high concentration of TiO<sub>2</sub> can actually lower the depth of solar light penetration, as the dosage of TiO<sub>2</sub> increases to enhance the photocatalysis rate (M et al. 2000). The other disadvantage of using TiO<sub>2</sub> powder is a requirement to separate TiO<sub>2</sub> powder from the treated water after finishing the treatment process (Borges et al. 2016) as the photoreaction occurs on the surface of the photocatalyst materials when the solar light is

irradiated on it. Therefore it is convenient to use an immobilized photocatalyst to a surface for the photocatalysis application for wastewater treatment. Among the immobilized photocatalyst fabricating techniques, thin-film deposition (TFD) is considered the most promising method to fabricate the photocatalyst on a substrate. As the photocatalyst surface is required for photo-reaction, so any substrate coated with thin-film of a photocatalyst may exhibit photocatalytic activities. This way, a wide range of materials can be employed as a substrate instead of using bulk photocatalyst materials. A wide range of thin-film deposition techniques has been applied on fabricating photocatalysts such as sol-gel, dip coating, spin coating, physical vapor deposition (PVD), chemical vapor deposition (CVD), and atomic layer deposition (Mavukkandy et al. 2020). Atomic layer deposition is considered a prominent TFD technique because the film fabricated by ALD is very uniform, conformal, repeatable, scalable, pin-hole free, and ultra-thin (Mavukkandy et al. 2020). Furthermore, ALD requires moderate pressure and low temperature, which favorable for fabricating thin film on temperature-sensitive materials such as polymers (Guo et al. 2017).

## **2.6 Atomic Layer Deposition**

Atomic layer deposition (ALD) is a vapor phase deposition technique modified from the chemical vapor deposition technique. ALD has several advantages and unique features that make it the most attractive and promising thin-film technique over others, such as chemical vapor deposition (CVD) and physical vapor deposition (PVD). ALD is characterized by sequential, self-limiting, and gas-surface deposition reactions. The self-limiting characteristics of ALD restrict the surface reaction to no more than a monolayer of a precursor. Thus the precursor can reach the depth of the substrate with sufficient precursor pulse times that allow the uniform coating on a three-dimensional substrate as well. Therefore the reaction cycles provide a uniform growth of the thin films even on high aspect ratio substrates, while the CVD and PVD cannot show the same level of uniformity of growing thin-film due to faster surface reactions and shadowing effects (Johnson et al. 2014). Another great advantage of ALD is the ability to control the thickness of the deposited thin film. As the layer-by-layer deposition has occurred during ALD, the thickness of the thin film can be adjusted by counting the ALD reaction cycles at the angstrom ( $10^{-10}$  m) level, which is a typical amount of deposition in a reaction cycle

(Johnson et al. 2014). Another promising feature of ALD is composition control. The thin-film such as a ternary oxide (Furlan et al. 2017), Zinc-Tin-oxide (ZTO) (Hultqvist et al. 2011), and SrTiO<sub>3</sub> (Kosola et al. 2003) can be deposited by ALD. Such films can be deposited and managed compositionally by adapting ALD 'super cycles', which are made up of multiple ALD processes (Johnson et al. 2014).

ALD technique is modified from CVD; thus mechanism of it has differences. The mechanism of ALD thin film growth has been shown in Figure 3. ALD thin film has been fabricated on a substrate in a very controlled manner. For deposition of the desired thin film on a surface, the substrate needs to have an appropriate functional group. Suppose it doesn't have sufficient groups, then a pre-functionalization might be necessary. The functionalized surface or the substrate is then placed in the ALD reactor under the medium vacuum (typically < 1 Torr) (Johnson et al. 2014). The temperature of an ALD reactor varies; however, it is usually lower than the CVD temperatures (in general < 300 °C). In ALD, chemical precursors vapors are introduced to the substrate in an alternating sequential manner. During the film formation of ALD, "A" precursor (Fig. 3) is pulsed with a specific pulse time according to the size of a reactor chamber or as instructed by the vendor. The gas precursors react with the substrate and form a monolayer, which is called a half-reaction or a half cycle. The unreacted or by-product produced from the "A" precursor reactions has been purged from the reactor chamber with the help of inert gas under a specific purging time. After that, the "B" precursor is pulsed to the substrate and reacts with previously formed monolayer, and fabricates a layer of desire thin-film, which is called a full reaction or full cycle. Later, inert gas has been purged to the reactor to remove unreacted precursor or by-product from the reactor chamber. The reactions have been carried out sequentially and self-limiting manner. The reaction cycles have been continued until the desired thickness of a thin-film has been achieved. The thickness of the thin film can be measured by counting the reaction cycle employ for depositing the thin film.

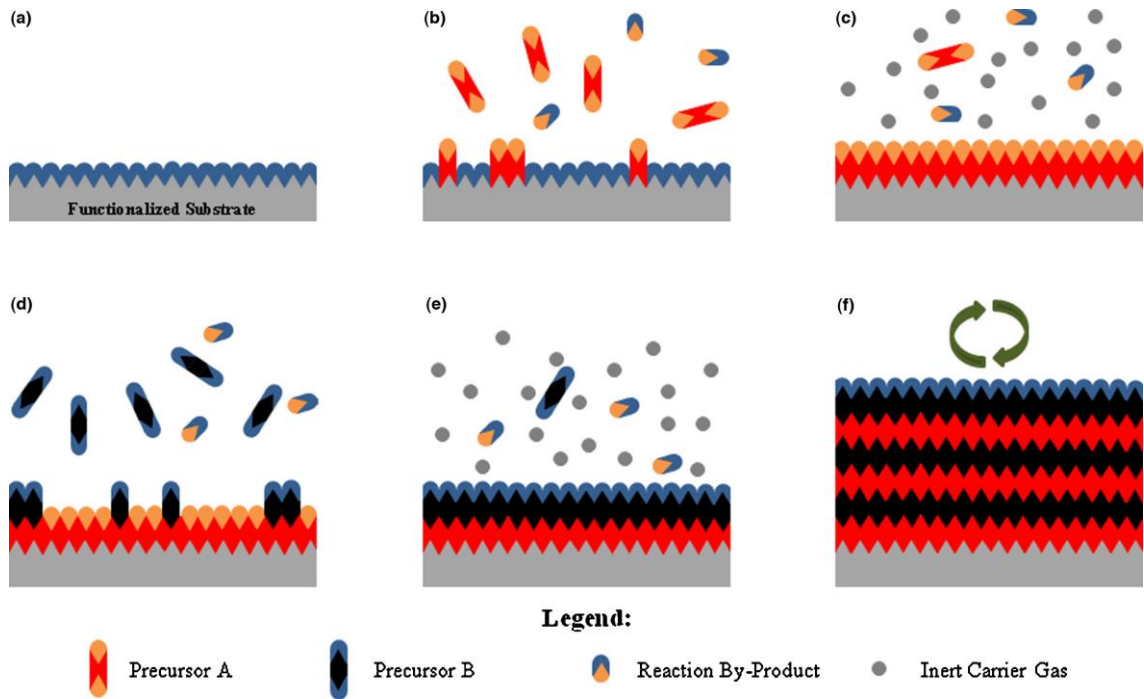


**Figure 3:** Thin-film growing mechanism of the atomic layer deposition technique (Johnson et al. 2014).

The ALD process parameters such as precursors pulsing time, inert gas purging time, precursor flux (vapor pressure), and growth temperature have a significant impact on thin-film growth. If the pulse time increases, the density of chemisorbed materials on the surface also increases, which leads to faster surface saturation on a substrate. If the pulse time is too short, may occur insufficient precursor molecules transport to the reaction chamber, resulting in an ununiformed thickness of thin-film (Ritala ve Leskela 2002). The precursor flux has a similar effect to pulse time in terms of thin-film growth. The growth rate per cycle may increase by only increase the pulsing time without changing the precursor flux rate (Ritala ve Leskela 2002). However, in the case of oxide ALD formation, the growth rate may increase by increasing H<sub>2</sub>O precursor flux than increasing the pulsing time of water precursor (Ritala ve Leskela 2002). The purge length is also another important process parameter of ALD. Inadequate purging may result in overlapping of precursor doses, resulting in a CVD like thin-film deposition and forming an ununiform thin-film deposition (Ritala ve Leskela 2002). The growth temperature is also one of the most important process parameters of ALD. There are several types of growth rates that may be occurred depending on the growth temperature. Outside the self-

limiting window of the temperature, the growth rate may increase or decrease. The growth rate may decrease at low temperatures due to the slow reaction rate and inadequate purging time. The growth rate may increase at low temperatures because of multilayer adsorption and the condensation of low vapor pressure precursors. Outside the self-limiting window of the temperature, the growth rate may increase or decrease too. The growth rate decreases at high temperature due to the desorption of the precursors, and increases at high temperature is caused by precursor decomposition ((Ritala ve Leskela 2002). There is a temperature range at a self-limiting region where the growth rate remains constant. The range of this temperature is called the temperature window. The temperatures in the temperature window is employed in ALD for uniform thin-film formation.

## **2.7 Photocatalytic ALD Thin Films**

The photocatalytic metal oxides such as TiO<sub>2</sub>, ZnO have been fabricated by ALD due to their uniform, conformal, and pin-hole free thin-films formation ability. Photocatalytic metal oxides have been deposited on different substrates via the atomic layer deposition technique. Promising photocatalytic activities have been found from ALD fabricated metal oxides on various substrates. As the photocatalytic activity of metal oxide has been greatly dependent on a surface area of metal oxide, it is assumed that ALD fabricated thin-film may utilize the highest surface area of metal oxide during the photocatalytic reaction compared to the other thin-film methods. A significant number of research works have been carried out on photocatalytic ALD metal oxide, and these researchers have found significant results. The first photocatalytic activity of an ALD TiO<sub>2</sub> thin-film was published in 2004. In this study, Pore *et al.* fabricated different thicknesses (60-150 nm) of TiO<sub>2</sub> thin-films at temperature 200-400 °C on a glass substrate via ALD. They demonstrated 70% methylene blue (concentration of 1x10<sup>-5</sup>M) photodegradation had been achieved under four hours of UV light irradiation from the 350 °C ALD coated TiO<sub>2</sub> thin film (B. V. Pore et al. 2004). In another article, Pore *et al.* illustrated that the TiO<sub>2</sub> ALD thin-films had been coated on soda-lime and borosilicate substrate using TiF<sub>4</sub> and H<sub>2</sub>O as the precursor for evaluating the photocatalytic activities (V. Pore ve Kivel 2008). Dey *et al.* fabricated ALD TiO<sub>2</sub> thin-films on carbon fiber and assessed the MB degradation under UV light (Kumar et al. 2011). N-doped TiO<sub>2</sub> ALD thin-film has been

fabricated on borosilicate glass and indium tin oxide (ITO)-coated glass substrates to assess the photocatalytic activities. The study elucidated that the N-doped TiO<sub>2</sub> had been exhibited less photocatalytic activities than undoped TiO<sub>2</sub> for the decomposing of the steric acid layer under UV light irradiation (V. Pore et al. 2006). Photocatalytic ZnO also has been fabricated by ALD. Di Mauro *et al.* have fabricated ZnO thin-films on polyethylene naphthalate (PEN) via ALD at low temperatures, and MB photodegradation has been observed (Di Mauro et al. 2016). Photocatalytic ALD ZnO also can be deposited on electrospun polymeric nanofibers via ALD. Kayaci *et al.* illustrated that the ZnO ALD thin-films have been deposited on electrospun nylon 66 fibers and achieved a significant photocatalytic activity to decompose the Rh-B solution under UV light irradiation for 24 hours (Kayaci et al. 2013). Jeong *et al.* have been fabricated ZnO shell on Ag core through ALD (Jeong et al. 2014). Ag-ZnO core-shell has been shown a promising photodegradation efficiency under UV irradiation. It can decompose 95% Rh-B, in only one hour of UV irradiation.

ALD is very a promising thin-film deposition technique with enormous potential in terms of material composition and substrate variety. It can deposit thin-film on the two-dimensional and three-dimensional substrates with high uniformity, conformity, and precise thickness control. Researchers have an interest in producing visible-light-induced photocatalyst thin-films for environmental application and renewable energy production. Thus, atomic layer deposition can be a great thin-film deposition technique for the researchers to fabricate visible-light-induced photocatalysts.

### 3. MATERIALS and METHODS

#### 3.1 Substrates Preparation

ALD thin films had been deposited on Glass fabrics (plain fabric, 200 g/m<sup>2</sup>, 0.15 mm of thickness from Hexel, Stamford, Connecticut, United States), 1 x 1 cm undoped silicon wafer (Nanography, Turkey), 2 x 2 cm fused quartz slide (Technical Glass Product, USA) and 2 x 2 cm glass slide. The glass fabrics had been conducted for the photocatalysis experiment, and other substrates were used for analyzing the characterization of thin films. The glass fabrics were used for ALD as received from the supplier, and other substrates were first immersed into acetone for 10 min. After that, substrates were placed under ethanol and kept there for 5 min and then rinsed with deionized (DI) water.

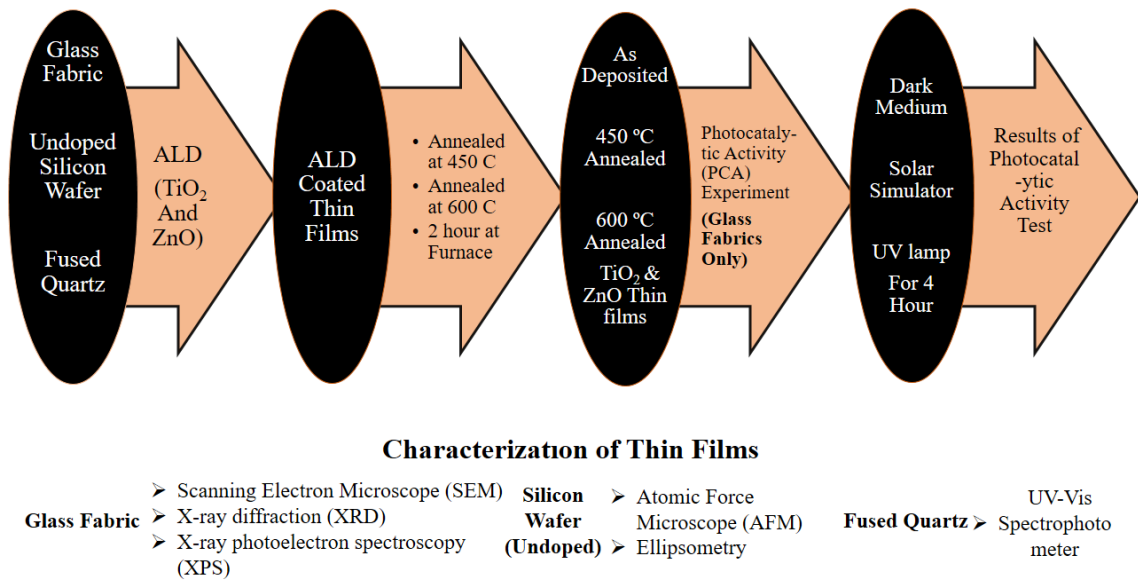


**Figure 4:** Experiment Flow Chart.

#### 3.2 Thin films Growth Parameters

Photocatalyst TiO<sub>2</sub> and ZnO ALD thin films had been deposited on the substrates by Savannah ALD system (Cambridge Nano Tech Inc. USA). Tetrakis (Dimethylamido) Titanium (TDMAT) (CAS # 3275-24-9, Sigma Aldrich) and H<sub>2</sub>O were used as the precursors of TiO<sub>2</sub>, and Diethyl Zinc (DEZ) (CAS # 557-20-0, Sigma Aldrich) and H<sub>2</sub>O were used as precursors of ZnO thin films during the ALD. High purity N<sub>2</sub> gas was used as the inert gas for carrying the reactive gases and byproducts. The reactor temperature of ALD was kept 150 °C for all samples, and the precursor temperature of TDMAT and DEZ was kept at 75 °C. The ALD reaction cycle recipe for TiO<sub>2</sub> thin film formation was

0.1s/ 20s/ 0.015s/ 20s (TDMAT pulsing/ N<sub>2</sub> purging/ H<sub>2</sub>O Pulsing/ N<sub>2</sub> purging) and for ZnO was 0.015s/ 20s/ 0.015s/ 20s (DEZ pulsing/ N<sub>2</sub> purging/ H<sub>2</sub>O Pulsing/ N<sub>2</sub> purging). The total ALD cycle of TiO<sub>2</sub> film formation was 250 and for ZnO thin film, it was 65 cycles to achieve the 10 nm ALD thin films for both photocatalysts. TiO<sub>2</sub> and ZnO thicknesses on the silicon wafer were confirmed using a variable angle spectroscopic ellipsometer (Spectral range: 200-2000 nm, J.A. Woollam Co., Inc. Lincoln Nebraska US.)



**Figure 5:** Savannah ALD system.

### **3.3 Annealing of ALD Thin films**

The substrates which were coated with TiO<sub>2</sub> and ZnO thin films were introduced for annealing. Annealing had been done under ambient conditions. The thin films had been annealed at 450 °C and 600 °C for two hours in an electric furnace. After finishing the duration of annealing, the furnace door was left open to cold down to the room temperature.

### **3.4 Photocatalytic Activity Experiment**

Photocatalytic activities of TiO<sub>2</sub> and ZnO ALD thin films had been evaluated by the degradation of methylene blue (MB) solution. The MB solution (CAS # 122965-43-9), ISOLAB, Germany) was prepared with DI water containing the molar concentration

$5 \times 10^{-5}$  M. The ALD coated glass fabrics had been cut down around  $5 \text{ cm}^2$  for photocatalytic activity test. After that, the ALD coated glass fabric was placed to 50 ml of MB solution in a beaker and kept the beaker under a dark cabinet for 30 min for absorption desorption equilibrium. Later photocatalytic activities of the thin films had been carried out under three medium such as dark medium, solar simulator (Model: SF-300-B, Sciencetech, Canada; 300W Xenon arc lamp USHIO Inc. Japan), and UV lamp (UVP Balk-Ray 365nm High-Intensity 100W, USA) irradiation for four hours. The distance between the light source and the surface of MB solution was 10 cm. The absorbance of MB was obtained by UV-Vis spectrophotometer (UV-3600, SHIMADZU, Japan). The highest absorbance of MB was observed at 664 nm of wavelength. Using the Lambert-Beer law  $A/A_0$  was taken equal to the  $C/C_0$  where  $A_0$  and  $C_0$  were the initial absorption and concentration of MB solution, and  $A$  and  $C$  were the absorption and concentration of MB at any given time. During the photocatalytic activity tests, the concentration variation of the MB solution was recorded as a function of time at 20 min, 40 min, 60 min, 120 min, 180 min, and 240 min. So, every given time interval small sample of MB solution was taken and measured the concentration using a UV-Vis spectrophotometer. The MB solution was agitated by a magnetic stirrer at the time of irradiation for maintaining a homogenous mixture of MB solution.

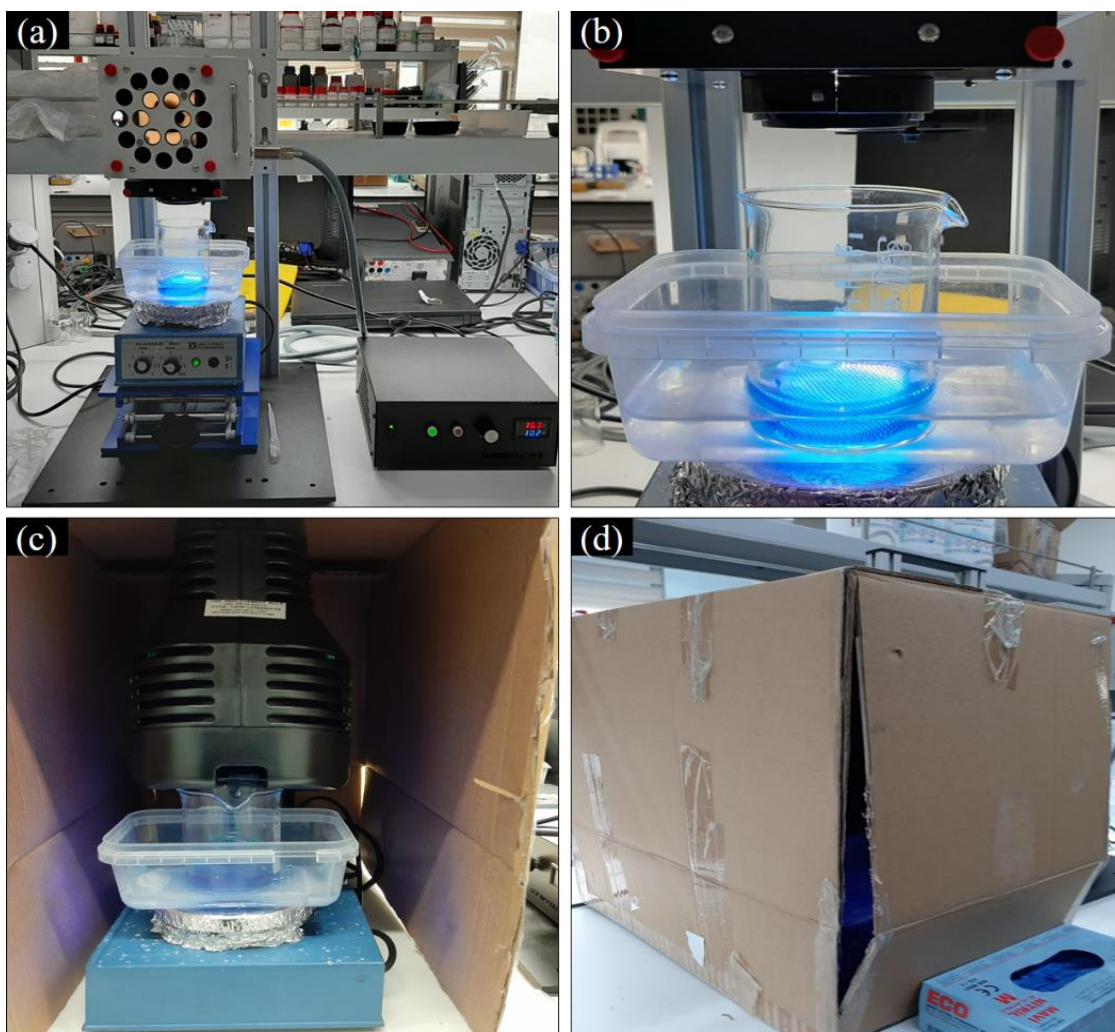


**Figure 6:** Photocatalytic Experiments Under (a) & (b) Solar Simulator and (c) & (d) Under UV Lamp.

### 3.5 Characterization of ALD Thin films

#### 3.5.1. Field Emission Scanning Electron Microscope (FESEM)

The morphology and microstructure of the ALD thin films deposited on glass fabrics were investigated by Field emission Electron Microscope (FESEM) (Zeiss / Gemini 300).  $1 \times 1 \text{ cm}^2$  samples were prepared for FESEM analysis. As the samples were not conductive, 15 nm of Au/Pd ultra-thin films had been deposited on the surface of the samples by sputtering methods to inhibit charging at the time of FESEM analysis. SEM images were taken in secondary electron mode using the voltage at 10 eV.

### 3.5.2 Atomic Force Microscope (AFM)

3-D surface morphology and surface roughness of ALD thin films were investigated by Atomic Force Microscope (AFM) (AFM, NanoMagnetics Instruments). ALD coated silicon wafers were employed to analyze AFM. A silicon cantilever with a typical tip (Techno Tip) radius < 10 nm was used to generate an AFM image. 4x4 μm<sup>2</sup> scan size was selected to produce an AFM image.

### 3.5.6 UV-Vis Spectrophotometer

Optical properties such as absorbance properties of ALD thin films were investigated by UV-Vis spectrophotometer (UV-3600, SHIMADZU, Japan). Absorbance was measured with the range between 200–700 nm of wavelength through the ALD coated fused quartz samples. The energy bandgap of the thin films was determined from the Tauc plot using absorbance data acquired from the UV-Vis spectrum and Tauc and Devid-Mott equation (Makula et al. 2018, Shkir et al. 2018). The Tauc and Devid-Mott equation,

$$(\alpha h\nu)^{1/n} = K (h\nu - E_g) \dots\dots\dots (3.1)$$

Here,  $\alpha$  is an absorption co-efficient,  $h\nu$  is the incident photon energy,  $K$  is the energy-independent photon energy, and  $E_g$  is the optical band gap energy of thin films. The exponent “n” the nature of electron transition from valance to the conduction band. For direct bandgap transition, the value of  $n = \frac{1}{2}$ , while indirect transition the value  $n = 2$ . Indirect transition has occurred for amorphous TiO<sub>2</sub> and anatase, so the  $n = 2$  (Shi et al. 2017), and for ZnO ALD thin films, the direct transition has occurred, so the value of  $n$  is  $\frac{1}{2}$  (Viezbicke et al. 2015). The wavelength (nm) data of corresponding absorbance data was converted into energy (eV) as explain below.

From Max Plank Equation, we know,

$$E_g = h\nu \dots\dots\dots (3.2)$$

Here,  $h$ = plank constant and  $\nu$ = frequency

$$\nu = \frac{c}{\lambda} \dots\dots\dots (3.3)$$

Here, C is the velocity of light, and  $\lambda$  is the wavelength of the incident photon.

Putting the  $v$  value into equation (2) we get,

$$E_g = \frac{hc}{\lambda} \dots\dots\dots(3.4)$$

$h = 6.62 \times 10^{-34}$  Js and  $C = 3 \times 10^8$  ms<sup>-1</sup>, Putting this value in equation (4) and we get,

$$E_g = \frac{6.62 \times 10^{-34} \text{ Js} \times 3 \times 10^8 \text{ ms}^{-1}}{\lambda} \dots\dots\dots(3.5)$$

Converting joule into eV ( $1 \text{ eV} = 1.602 \times 10^{-19}$  J) and simplify the equation we get,

$$E_g = \frac{6.62 \times 10^{-34} \times 3 \times 10^8 \text{ eV m}}{\lambda \times 1.602 \times 10^{-19}}$$

$$E_g = \frac{1239.3 \times 10^{-9} \text{ eV m}}{\lambda}$$

$$E_g = \frac{1239.3 \times 10^{-9} \text{ eV nm}}{\lambda \times 10^{-9}}$$

$$E_g = \frac{1239.3 \text{ eV nm}}{\lambda} \dots\dots\dots(3.6)$$

The X-axis of Tauc was plotted using equation (3.6), adding the wavelength ( $\lambda$ ) value in it.  $(\alpha h\nu)^n$  value of Tauc equation was used as Y-axis for plotting Tauc plot. As the equation, we were needed to find the absorbance coefficient ( $\alpha$ ). Beer-Lambert law was used to determine the find absorbance coefficient ( $\alpha$ ) explained below.

In figure 7,  $I_0$  is the incident light,  $I$  is the transmitted light,  $\alpha$  is the absorbance coefficient, and  $l$  is the path-length of light in which absorbance takes place. From the Beer-Lambert equation, we get,

$$I = I_0 e^{-\alpha l}$$

$$\frac{I}{I_0} = e^{-\alpha l}$$

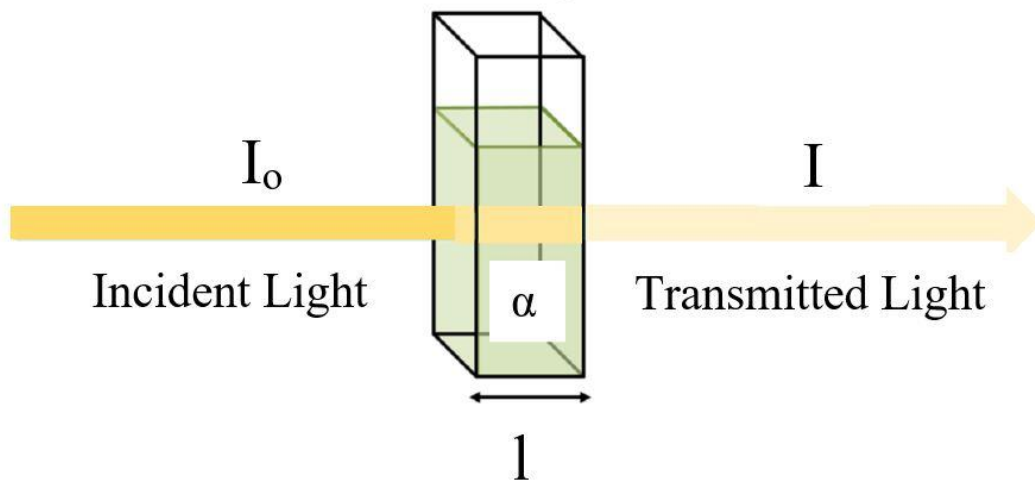


**Figure 7:** Beer-Lambert law of Absorption.

Taking Log on both sides,

$$\begin{aligned} \log \left(\frac{I}{I_0}\right) &= \log e^{-\alpha l} \\ \log \left(\frac{I}{I_0}\right) &= -\alpha l \log e \\ \log \left(\frac{I_0}{I}\right) &= \alpha l \log e \dots\dots\dots(3.7) \end{aligned}$$

As Absorbance,  $A = \log \left(\frac{I_0}{I}\right)$ . So, we can get from equation (7)

$$\begin{aligned} A &= \alpha l \log e \\ \alpha &= A \frac{1}{l \log e} \end{aligned}$$

Here,  $\log e = 0.4343$  and  $l$  = the thickness of ALD thin films (Pal et al. 2017, Purohit et al. 2015).

$$\begin{aligned} \alpha &= A \frac{1}{l \times 0.4343} \text{ cm}^{-1} \\ \alpha &= 2.303 \times A l \text{ cm}^{-1} \dots\dots\dots(3.8) \end{aligned}$$

Absorbance (A) values were received from UV-Vis Spectrum and input into the equation (3.8). Later multiply with  $E_g$  value from equation (3.6) and plotted the Y-axis of Tauc's Plot against the X-axis from the equation (3.6). After plotting the Tauc's plot, the bandgap ( $E_g$ ) value of ALD thin films was determined from the plot keeping the  $(\alpha h\nu)^n$  value zero and find the intersection point on X-axis on the plot. The intersection point represents the bandgap energy of the particular thin films or materials. The Tauc's plot results are explained in the "result and discussion" section elaborately.

### **3.5.7 X-ray Diffractometer Analysis (XRD)**

The crystallinity of ALD thin films on glass fabric was studied using X-ray Diffractometer (XRD) (High-resolution Bruker/D8 Advance system) using Cu K $\alpha$  radiation (Cu tube, 1.54 Å). XRD analysis was carried out on ALD coated glass fabrics.  $\theta$ -2 $\theta$  scans were used to measure the samples. Baseline correction and smoothness of XRD patterns have been edited by Origin pro-2019 software.

### **3.5.8 X-ray photoelectron spectroscopy (XPS)**

The elemental composition and element bonding state of ALD thin films were analyzed using X-ray photoelectron spectroscopy (XPS, K-Alpha Thermo Scientific) using monochromatic Al K $\alpha$  as an X-ray source. Photon energy of X-ray source was 1486.6 eV. 400  $\mu$ m were used as spot size for XPS analysis. The peak of XPS spectra was fitted using the Gaussian-Lorentzian function via XPSPeak41 software.

## 4. RESULTS and DISCUSSION

### 4.1 FESEM Image of ALD TiO<sub>2</sub> and ZnO Thin Films

Figure 8 represents the FESEM image of ALD coated glass fabrics and pristine glass fabric. Figure 8 (a) and (b) represents the “as-deposited” TiO<sub>2</sub> and ZnO ALD thin films, respectively. Figure 4 (c) and (d) represent the 450 °C annealed TiO<sub>2</sub> and ZnO ALD thin films, respectively. Figure 8 (e) and (f) represent the 600 °C Annealed TiO<sub>2</sub> and ZnO ALD thin films, respectively as well, and figure 8 (g) represents the pristine glass fabrics. Inset images present in each FESEM image illustrate the 4 μ scan area of the sample, and the main image scan area is 300 nm. It is seen from the FESEM image that the thin films are homogeneously and uniformly coated on the surface of the glass fibers in comparison with the pristine glass fabric. The “as-deposited” TiO<sub>2</sub> thin films represent in figure 8(a) is amorphous because of not appearing any crystal grain of TiO<sub>2</sub> films. In literature, it is reported that TiO<sub>2</sub> ALD thin films grown at 190 °C or below it is amorphous (Xie et al. 2007). For 450 °C annealed (Fig 8 (c)) and 600 Annealed TiO<sub>2</sub> (Fig 8 (e)), we can observe the morphological change of the surface of the thin-films. From the literature, it is well known that the amorphous phase of TiO<sub>2</sub> thin films has been transformed into crystal anatase phase at annealed temperature range 400 °C to 500 °C and higher annealing temperature range 600 °C to 900 °C can lead to rutile phase (Dang et al. 2014, Lee et al. 2013). From the FESEM image of “450 °C annealed TiO<sub>2</sub>,” we may not clearly understand the crystal grain of the anatase phase. From the “600 °C annealed TiO<sub>2</sub>” FESEM image, we can understand the phase transformation has been occurred due to annealing. We assume that the low thickness (10 nm) of TiO<sub>2</sub> ALD thin films may be the reason not to get a precise image of the crystal grain of the thin films in the FESEM image. From FESEM images of ZnO ALD thin films, significant morphological changes may have observed from the surface of the thin films. Figure 8 (b), (d), and (f) are represented “as-deposited,” 450 °C and 600 °C annealed ZnO ALD thin films, respectively. Hexagonal wurtzite crystal grains have been observed on the surface of all ZnO ALD thin films. In literature, the crystal grain size of the ZnO ALD thin films is increased as the increased of annealing temperature (Cao et al. 2015). However, It is hard to conclude on FESEM image regarding grain size variation among the “as-deposited” and annealed ZnO thin

films. As mention before, the low thickness of (10 nm) ZnO ALD thin films may be the reason for not get a precise image at FESEM.

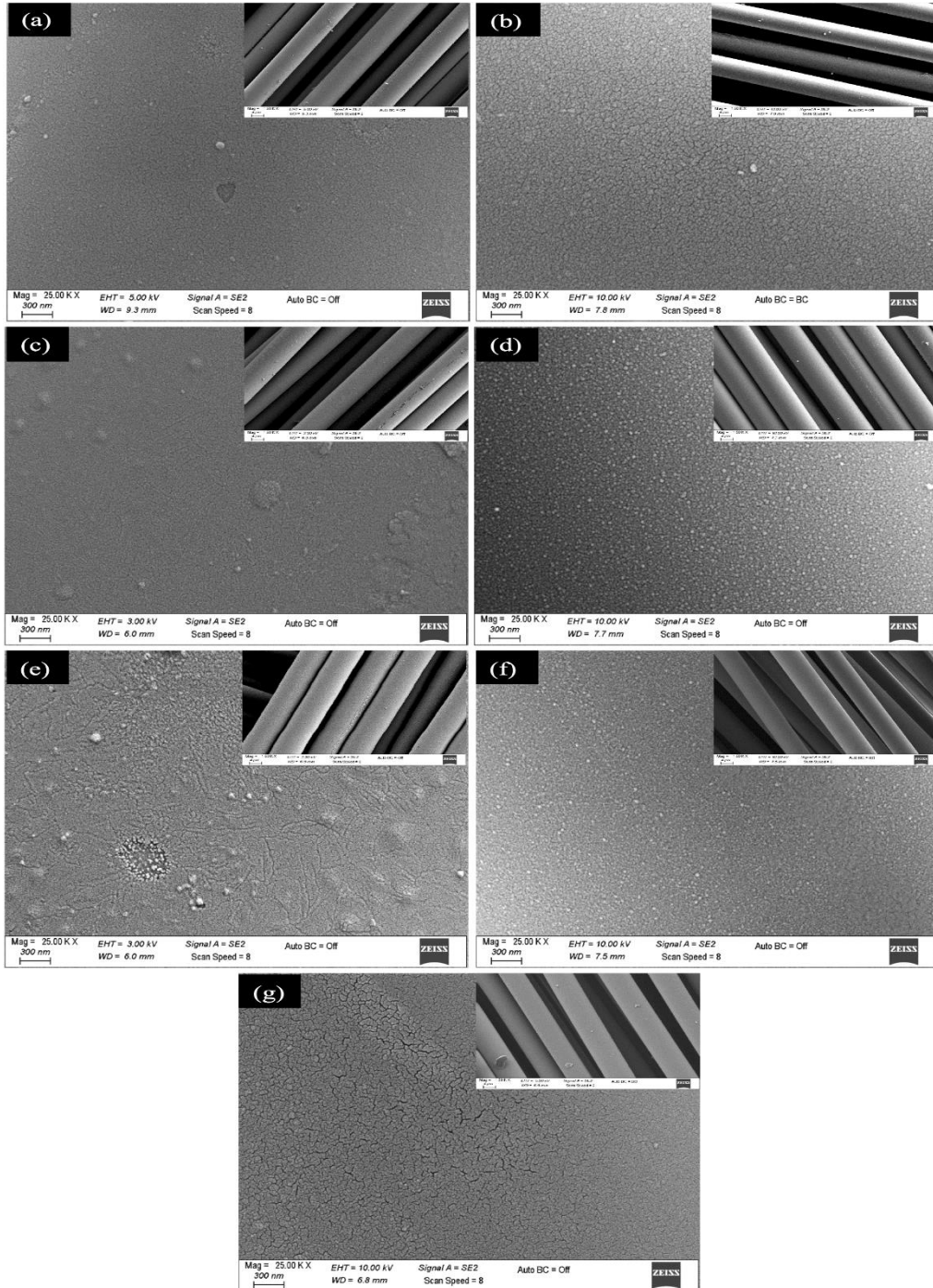


**Figure 8:** FESEM Image of “as deposited”TiO<sub>2</sub> (a) and ZnO (b); 450 °C Annealed TiO<sub>2</sub> (c) and ZnO (d); 600 °C Annealed TiO<sub>2</sub> (e) and ZnO (f) ALD thin films & Pristine Glass Fabric (g).

## 4.2 AFM Analysis of ALD Thin Films

3-D morphology and root mean square (rms) roughness of ALD thin films have been illustrated in figure 9. Figure 9 (a), (c), and (e) are represented the 3-D image including rms roughness of “As deposited,” 450 °C and 600 °C annealed TiO<sub>2</sub> ALD thin films and figure 9 (b), (d), and (f) represent the “As deposited,” 450 °C and 600 °C annealed ZnO ALD thin films respectively. From figure 9, we can clearly see that the rms roughness of the films increased for both TiO<sub>2</sub> and ZnO ALD thin films when increased in annealing temperature. The rms roughness of as-deposited, 450 °C and 600 °C annealed TiO<sub>2</sub> thin films are 0.1463, 0.2454, and 0.4402, respectively. In literature, it is reported that rms surface roughness of TiO<sub>2</sub> ALD thin films had been increased as the increased in annealing temperature (Dang et al. 2014). And the rms roughness of “as-deposited” ZnO, 450 °C and 600 °C annealed ZnO ALD thin films are 0.4815, 1.2699, and 1.3051, respectively. In the literature, we also found the same results; that is, the rms roughness of ZnO ALD thin film had been increased with the increased in annealing temperature (Yen et al. 2011).

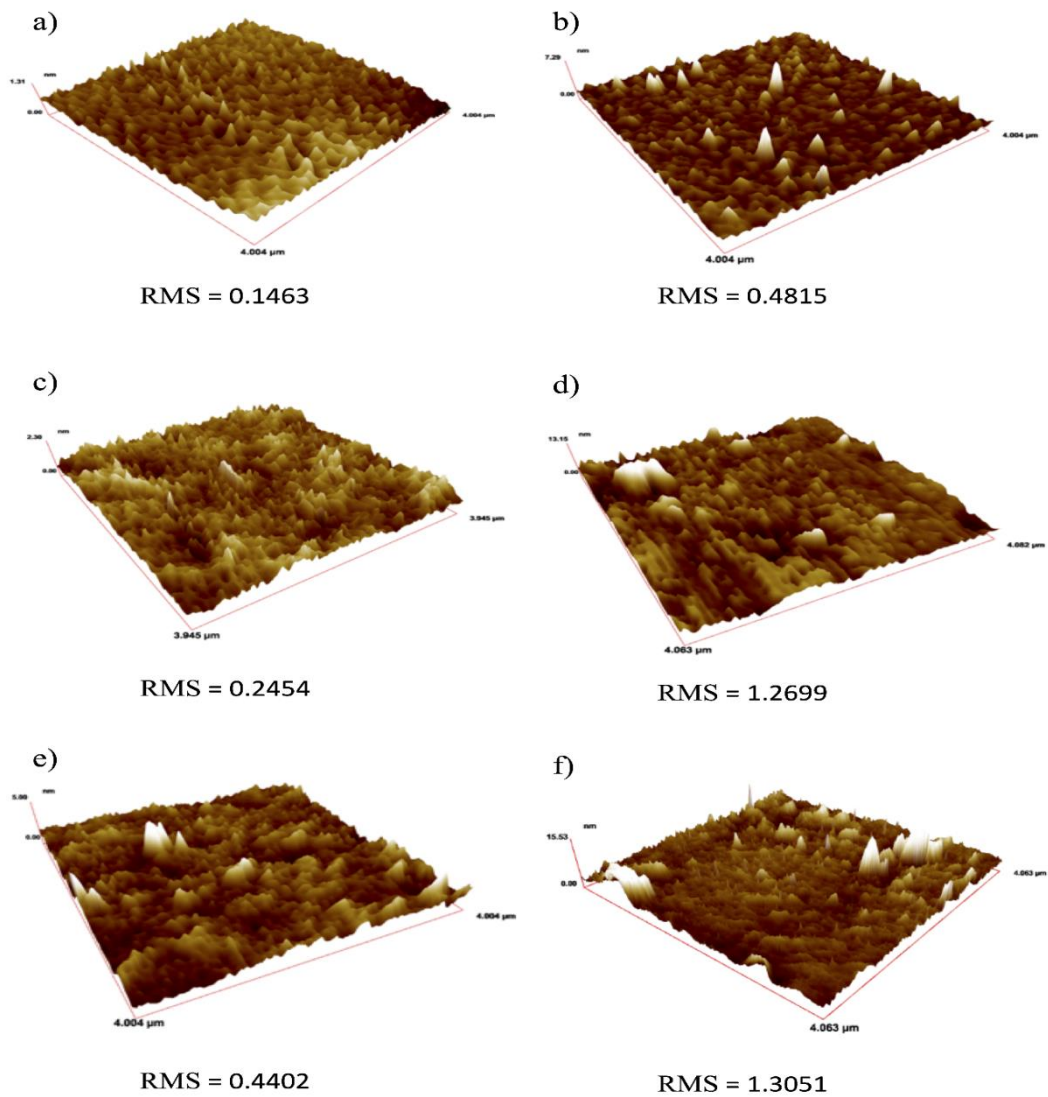


**Figure 9:** AFM Image of “as deposited”TiO<sub>2</sub> (a) and ZnO (b); 450 °C Annealed TiO<sub>2</sub> (c) and ZnO (d); 600 °C Annealed TiO<sub>2</sub> (e) and ZnO (f) ALD thin films.

### 4.3 XPS Analysis of ALD Thin Films

Elemental analysis of ALD thin films was carried out by X-ray photoelectron spectroscopy (XPS). Survey spectra of TiO<sub>2</sub> and ZnO and their different annealed ALD thin films along with pristine fabric have been presented in figure 10 (a) and (b), respectively. From the XPS spectrum of pristine fabric, we can identify the Si, Ca, Al, N, C, and O peak at binding energy 102.3 eV, 347.97 eV, 74.23 eV, 400.82 eV, 285.05, and 531.92 eV, respectively. Si, Ca, and Al have come from SiO<sub>2</sub>, CaO, and Al<sub>2</sub>O<sub>3</sub>, which were the raw materials used to manufacture E-glass fabric (Ku-Herrera et al. 2015).

Usually, XPS spectra have shown C 1s peak as a contaminant if the sample exposes to air. The O 1s is also a common peak that has been found in XPS if any kind of oxide materials or a layer of oxidized substance is present, and a little portion adventitious C may be oxidized, which can lead to an addition of some O as well (Shah et al. 2018). In figure 10 (a), we can observe that the Ti 2p peak at binding energy around 459 eV along with other peaks that are present in pristine glass fabric except for the N 1s peak. N 1s peaks are disappeared at annealed TiO<sub>2</sub> ALD thin films implying that N<sub>2</sub> impurity was removed during annealing. In figure 10 (b), we can see that Zn 2p<sub>3/2</sub> and Zn 2p<sub>1/2</sub> peaks are observed around 1022 eV and 1045 eV, respectively. It is also noticed that C 1s and O 1s peaks are seen in both “as-deposited” and annealed ZnO ALD thin films. Ca 2p, Al 2p and N 1s peaks are not seen in both “as-deposited” and annealed ZnO ALD thin films. Interestingly Si 2p peak has not been seen in “as-deposited” and 450 °C ZnO ALD thin films XPS spectra but only seen at 600 °C annealed ZnO ALD thin films. We assumed that deformation of glass fabric at 600 °C might have happened, which can be a reason to appear the Si 2p peak at 600 °C annealed ZnO ALD thin films. The structural deformation of glass fabrics may have happened at 600 °C as the technical report of glass fabrics stated that it could approximately retain 25% of its initial strength at 540 °C.

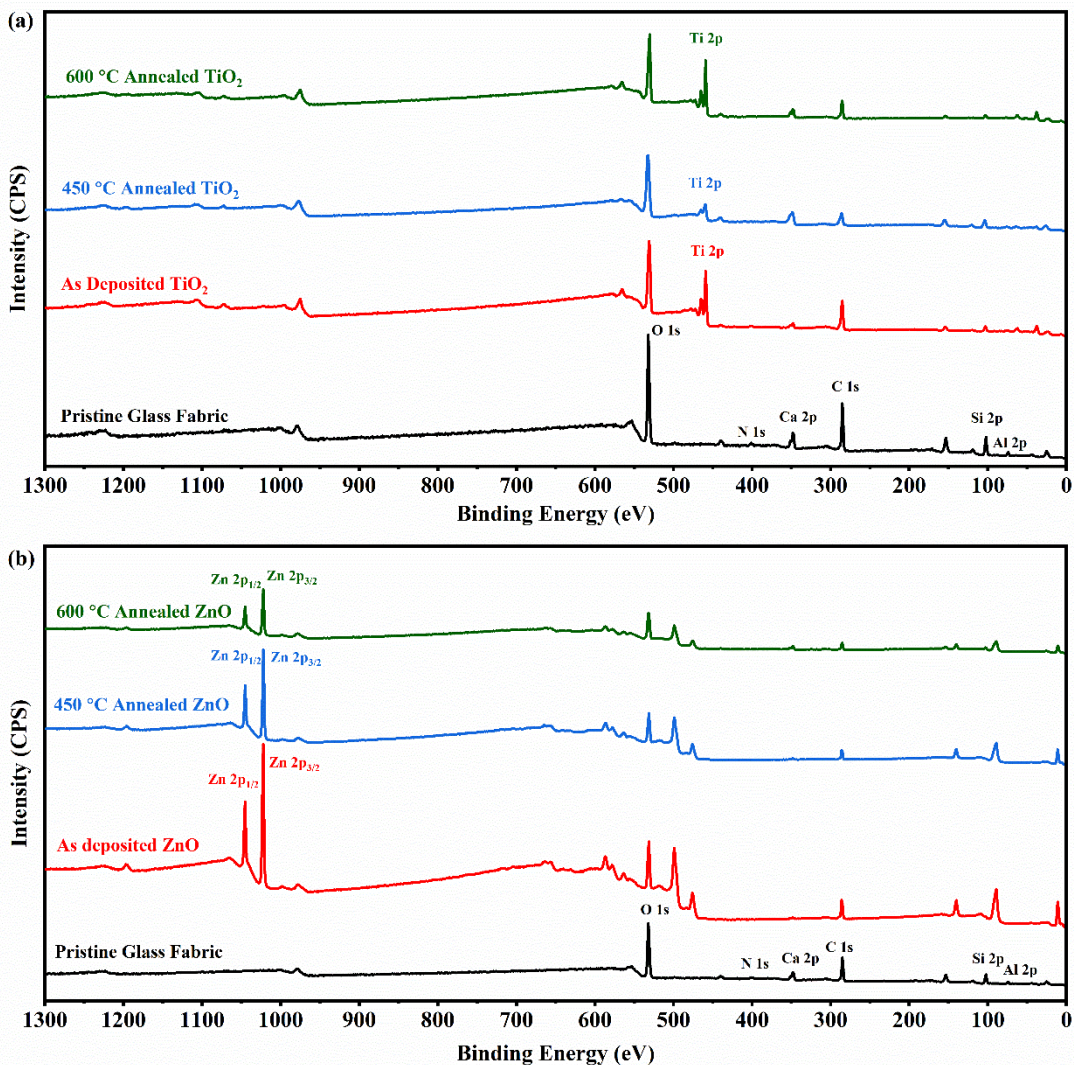


**Figure 10:** XPS Survey Spectra of TiO<sub>2</sub> (a) and ZnO ALD Thin film.

High-resolution XPS spectra of C 1s, O 1s, Ti 2p, and Zn 2p of TiO<sub>2</sub> and ZnO and their annealed ALD thin films have been presented in Figures 11, 12, and 13, respectively. All the XPS spectra were fitted by using Gaussian/Lorentzian function, and all the binding energy value was calibrated by using the C 1s signal to 285 eV (Kang et al. 2018). High-resolution XPS spectra of C 1s of “as-deposited” and annealed TiO<sub>2</sub> and ZnO ALD thin films are shown at figure 11 (a-f). In the figure, we can see that the C 1s peak was contributed to three peaks such as C-C, C-O, and C=O, both “as-deposited” and annealed TiO<sub>2</sub> (Gebhard et al. 2016, Jnido et al. 2019, Kang et al. 2018). For ZnO as-deposited and annealed ALD thin films, we are noticed only C-C and C=O peak. As we calibrated C-C

to 285 eV, so binding energy (BE) of C-C both TiO<sub>2</sub> and ZnO “as-deposited” and their annealed thin films are 285 eV. BE of C-O bond of “as-deposited, 450 °C and 600 °C annealed are 286.42 eV, 286.12 eV, and 285.74 eV, and for C=O the BE are 288.56 eV, 288.12 eV and 288.88 respectively. From figure 11 (a), (c), and (e), we can observe that BE variation of C-O and C=O “as-deposited’ and annealed TiO<sub>2</sub> thin films. From figure 11 (b), (d), and (e) we can see that BE of C=O of “as-deposited”, 450 °C annealed and 600 °C annealed ZnO ALD are 288.53 eV, 288.42 eV, 288.12 eV respectively. BE of C=O of as-deposited ZnO thin films observe highest in comparison to annealing ZnO thin films.

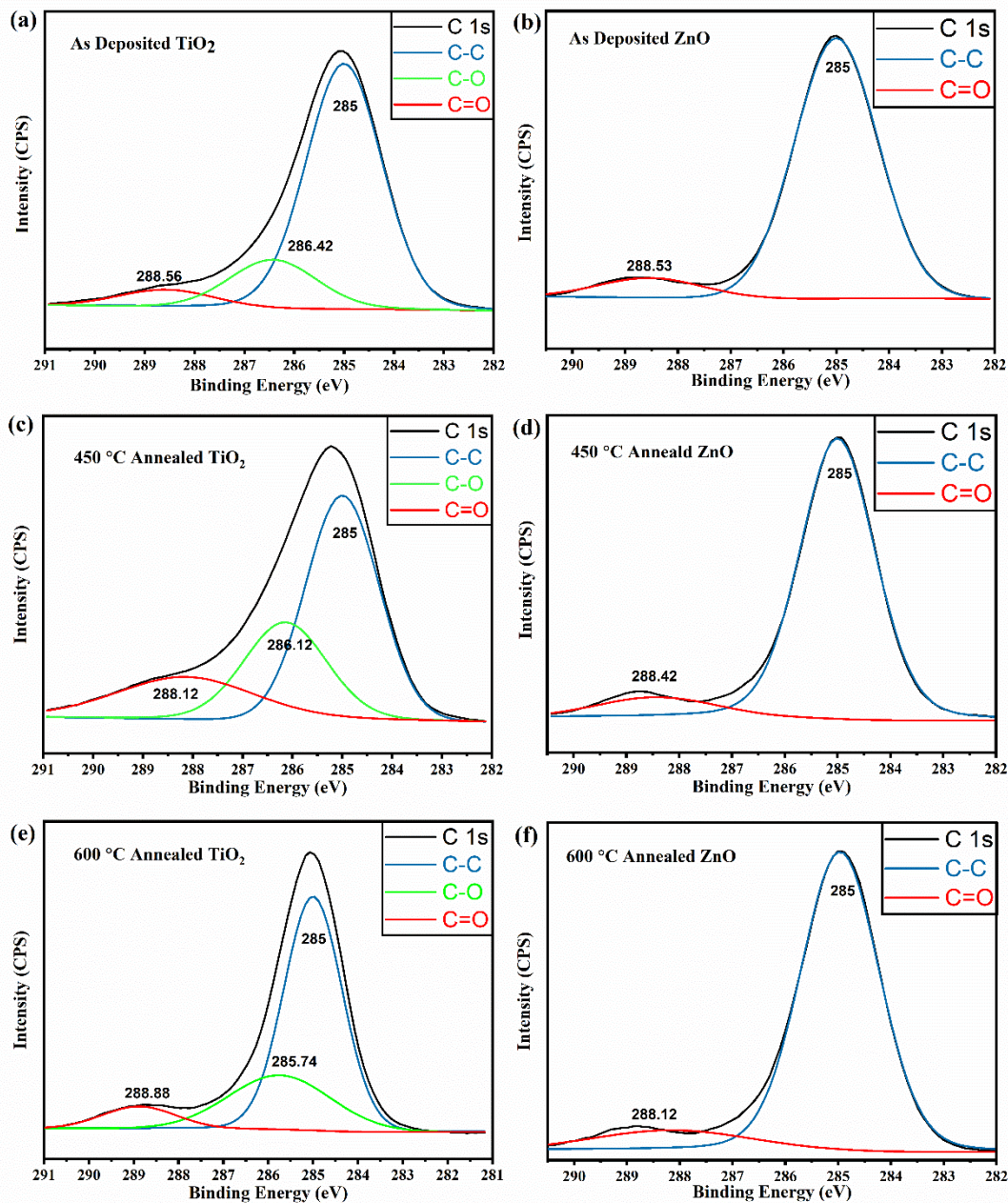


**Figure 11:** High-resolution C 1s XPS spectra of “as deposited”TiO<sub>2</sub> (a) and ZnO (b), 450 °C annealed TiO<sub>2</sub> (c) and ZnO (d), 600 °C annealed TiO<sub>2</sub> (e) and ZnO (f) ALD thin films.

The high-resolution O 1s spectra of TiO<sub>2</sub> and ZnO ALD thin films are depicted in figure 12. The high-resolution O 1s spectra of as-deposited 450 °C and 600 °C annealed TiO<sub>2</sub> thin films are presented at Figures 12 (a), (c), and (e), respectively. From figure 12, we see that the O 1s spectra were deconvoluted into three peaks, such as Ti-O, Ti-OH, and C-O, at different binding energy for various samples (Gebhard et al. 2016, Jnido et al. 2019, Kang et al. 2018). In the figure, we can see that, BE of Ti-O bond of as-deposited, 450 °C and 600 °C annealed are 530.06 eV, 530.22 eV, and 529.97 eV; BE of Ti-OH bond of as-deposited, 450 °C and 600 °C annealed are 531.62 eV, 531.98 eV, and 531.52 eV; BE of C-O bond “as-deposited”, 450 °C and 600 °C annealed are 533.27 eV, 533.03 eV and 532.94 eV, respectively. High-resolution spectra of “as-deposited,” 450 °C and 600 °C annealed ZnO ALD thin films are illustrated at 12 (b), (d), and (f), respectively. Here also we can observe that the O 1s spectrum is deconvoluted into three peaks such as Zn-O, oxygen deficiency, and O-H that is well reported in the literature (Jiang et al. 2017, Junpeng Wang et al. 2012, Y. H. Wang et al. 2016). Zn-O peak has been seen at lower BE 530.47 eV, 530.14 eV, and 530.26 eV for “as-deposited,” 450 °C and 600 °C annealed ZnO ALD thin films, respectively. The peak of O-H has been observed at higher BE 532.15 eV, 532.04 eV, and 531.8 eV corresponding to “as-deposited,” 450 °C annealed and 600 °C annealed ZnO ALD thin films, respectively. The O-deficiency peak has only been seen at “as-deposited,” and 450 °C annealed ZnO ALD thin films corresponding BE are 531.62 eV and 531.37 eV, respectively. The O-deficiency peak has been disappeared at annealed 600 °C ZnO thin films attributed that the O vacancy (V<sub>o</sub>) of the ZnO thin films were filled with free oxygen present in wurtzite structure during annealing (Jiang et al. 2017). In the literature, it is reported that the oxygen vacancy (V<sub>o</sub>) of ZnO thin films was decreased at high annealed temperature (Jiang et al. 2017, Junpeng Wang et al. 2012, Y. H. Wang et al. 2016). It is also reported that the carrier concentration of ZnO thin films was reduced as the decreased in concentration of oxygen vacancy (V<sub>o</sub>) (Jiang et al. 2017, Y. H. Wang et al. 2016).

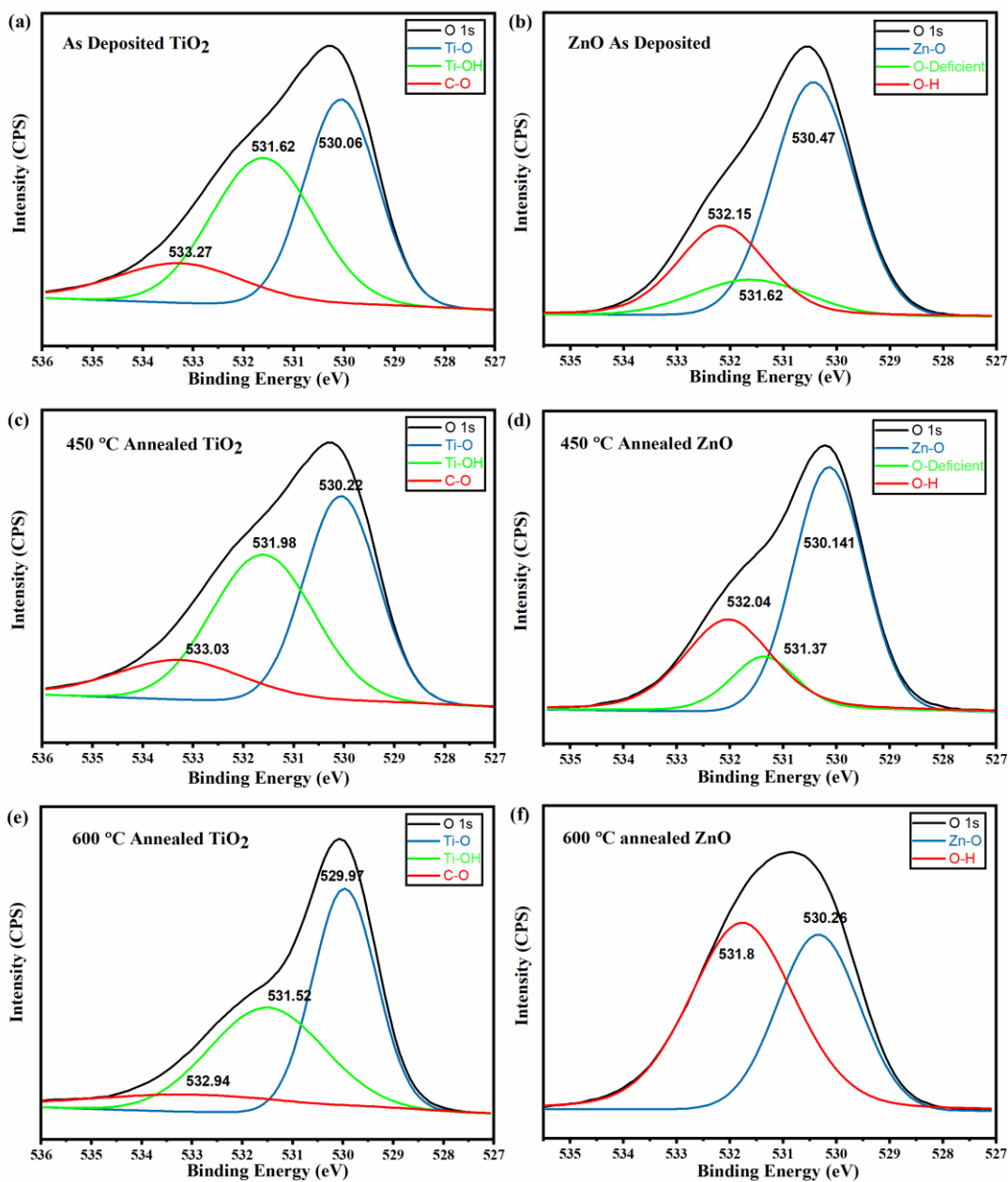


**Figure 12:** High-resolution O 1s XPS spectra of “as deposited”TiO<sub>2</sub> (a) and ZnO (b), 450 °C annealed TiO<sub>2</sub> (c) and ZnO (d), 600 °C annealed TiO<sub>2</sub> (e) and ZnO (f) ALD thin films.

High-resolution 2p doublet spectra of “as-deposited” TiO<sub>2</sub> and ZnO and their various annealed ALD thin films are depicted in figure 13. Figure 13 (a), (c), and (e) are presented “as-deposited,” 450 °C and 600 °C annealed TiO<sub>2</sub> ALD thin films, respectively. And figure 13 (b), (d), and (f) are represent the “as-deposited” 450 °C and 600 °C annealed

ZnO ALD thin films, respectively. The XPS spectra of “as-deposited,” 450 °C and 600 °C annealed TiO<sub>2</sub> ALD thin films, 2p doublet of Ti named Ti2p<sub>1/2</sub> and Ti2p<sub>3/2</sub> are observed that evidence that the presence of Ti on the thin films meaning that TiO<sub>2</sub> ALD was successfully deposited on glass fabrics. In the case of ZnO thin films, we also notice the doublet Zn 2p named Zn2p<sub>1/2</sub> and Zn2p<sub>3/2</sub> are observed in all ZnO ALD thin films, also indicate that ZnO ALD thin films were successfully deposited on the glass fabric.

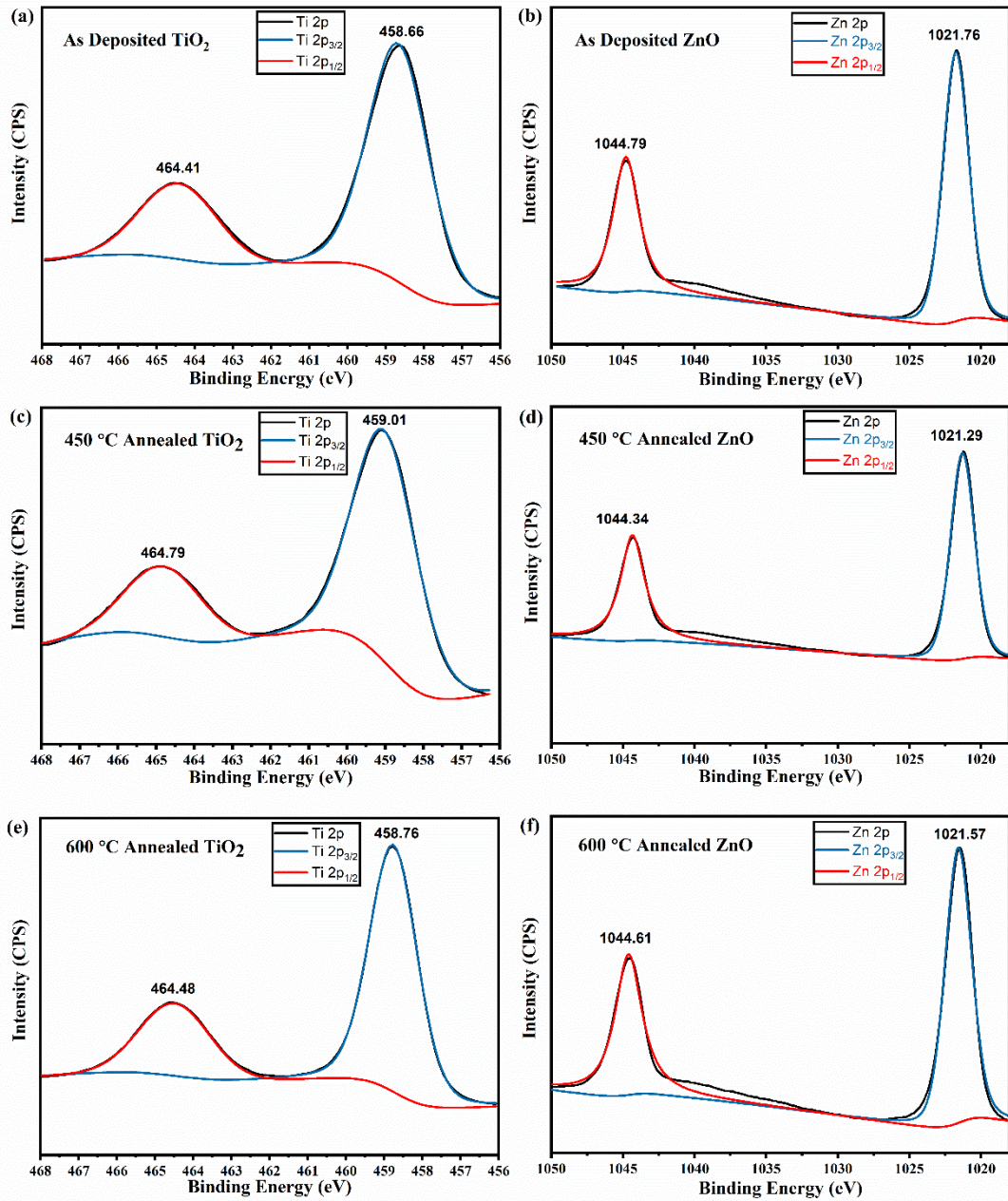


**Figure 13:** High-resolution 2p XPS spectra of “as deposited”TiO<sub>2</sub> (a) and ZnO (b), 450 °C annealed TiO<sub>2</sub> (c) and ZnO (d), 600 °C annealed TiO<sub>2</sub> (e) and ZnO (f) ALD thin films.

#### 4.4 XRD Pattern of ALD Thin Films

XRD patterns of TiO<sub>2</sub> and ZnO ALD thin films and their different annealed thin films have been illustrated in figure 14 (a) and (b), respectively. Miller index (hkl) of ALD thin

films has been determined by using JCPDS card. Anatase JCPDS card no 00-021-1272 was used to determine the characteristic crystal peak of the anatase phase of  $\text{TiO}_2$ , and JCPDS card no 00-021-1276 was used for the rutile phase of  $\text{TiO}_2$ . Hexagonal wurtzite crystal structure of ZnO ALD thin films was determined by using JCPDS card no 00-036-1451. From the XRD pattern of pristine glass fabric (fig 14 (a) and (b)), we can see that the pattern represents the amorphous structure of glass fabrics, although a little wave has been seen on the pattern, which may be originated from the component or impurity presents in the glass fabrics. XRD pattern of “as-deposited”  $\text{TiO}_2$  thin films from figure 14 (a), we can see that an amorphous phase of  $\text{TiO}_2$  is being observed. It is well known in the literature that the  $\text{TiO}_2$  thin films grown at a temperature below  $190\text{ }^\circ\text{C}$  in ALD was amorphous (Xie et al. 2007). XRD pattern of  $450\text{ }^\circ\text{C}$  annealed  $\text{TiO}_2$  thin film, and we can clearly see that the diffraction peak of anatase phase of  $\text{TiO}_2$  has been observed at  $25.28^\circ$ ,  $48.05^\circ$ ,  $55.06^\circ$  corresponding (hkl) index (101), (200), (211) respectively according to JCPDS card no 00-021-1272. The similar results of  $450\text{ }^\circ\text{C}$  annealed  $\text{TiO}_2$  ALD thin films had been well reported in the literature (Dang et al. 2014, Xie et al. 2007). It is interestingly seen that a little rutile crystal peak (110) has been observed at  $27.5^\circ$  too, although the peak is not sharp. In the XRD pattern of  $600\text{ }^\circ\text{C}$  annealed  $\text{TiO}_2$ , we can observe that both anatase and rutile crystal peaks have been seen. Anatase characteristic peaks such as (101), (200), and (211) have been observed at  $25.28^\circ$ ,  $48.05^\circ$ , and  $55.06^\circ$ , and rutile characteristic peaks such as (110) and (002) have been observed at  $27.5^\circ$  and  $62.72^\circ$  respectively. Moreover, the peaks are sharpened and high in intensity compare to  $450\text{ }^\circ\text{C}$   $\text{TiO}_2$  thin films. It is implied that the  $\text{TiO}_2$  thin annealed at  $600\text{ }^\circ\text{C}$  is more crystalline in nature, and phase transformation has occurred as well at the time of annealing. It is well arguable in the literature that the phase transformation had occurred at high annealing temperatures (Dang et al. 2014). XRD pattern of “as-deposited” ZnO and different annealed ALD thin films have been illustrated in figure 14 (b). From figure 14 (b), we can see that the hexagonal wurtzite crystal structure of ZnO ALD has been observed in all ZnO ALD thin films, including annealed thin films. The characteristic peaks of hexagonal wurtzite crystal structure such as (100), (002), (101), (102), (110), (103) have been observed at  $31.77^\circ$ ,  $34.42^\circ$ ,  $36.25^\circ$ ,  $47.54^\circ$ ,  $56.6^\circ$ ,  $62.86^\circ$  respectively. It is evident that the hexagonal wurtzite structure of ZnO ALD thin films had been successfully deposited on the surface of glass fiber.  $450\text{ }^\circ\text{C}$  annealed ZnO thin films have

been shown the highest crystallinity in comparison to other thin films. However, the crystallinity of the thin films had been decreased when it was annealed at 600 °C. In the literature, it is reported, the crystallinity of ZnO ALD thin films was increased as increased in annealing temperature (Cao et al. 2015, Tian et al. 2015, Yen et al. 2011). So, we assume that the decrease of crystallinity of 600 °C annealed ZnO thin films has resulted from glass fabrics. The structural deformation of glass fabrics may have happened at 600 °C as the technical report of glass fabrics stated that it could approximately retain 25% of its initial strength at 540 °C. The small peaks or noise which are not related to the corresponding thin films peak at XRD pattern may be originated from the element of glass fabric as the peaks have been seen at XRD pattern of pristine fabrics.

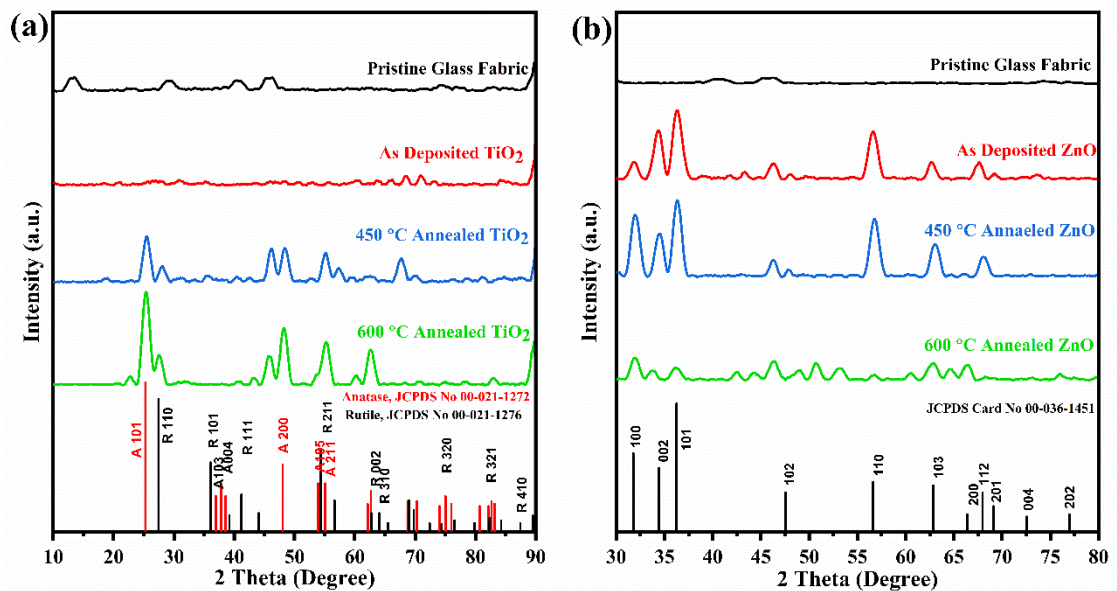


**Figure 14:** XRD pattern of TiO<sub>2</sub> (a) and ZnO ALD thin films.

#### 4.5 UV-Vis Absorbance Spectra and Bandgap Analysis

UV-Vis absorption spectra of TiO<sub>2</sub> and ZnO ALD thin films are represented at figure 15. The UV-Vis spectra were taken within the wavelength range between 200 to 700 nm for both TiO<sub>2</sub> and ZnO thin films. Figure 15 (a) and (b) represents the absorption spectra of “as-deposited,” 450 °C and 600 °C annealed TiO<sub>2</sub> and ZnO ALD thin films with black, blue, and red spectra, respectively. From figure 15 (a) we can see that a strong optical absorption edge has been observed at wavelength range 320 – 265 nm for “as-deposited”

and different annealed TiO<sub>2</sub> ALD thin films. The strong optical absorption edge for “as-deposited” and different annealed ZnO ALD thin films has been observed at the wavelength range 390 – 200 nm. Di Maura et al. was found similar optical absorbance spectra of ZnO ALD thin films (Di Mauro et al. 2016). From the strong absorption edge range of both TiO<sub>2</sub> and ZnO thin films, it can be concluded the films could absorb UV light and generate electron-hole on the surface of the thin films. In figure 15 (a), it is also observed that the highest blue shift has been exhibited on the 600 °C annealed TiO<sub>2</sub> thin films in comparison to “as-deposited” and 450 °C annealed TiO<sub>2</sub> films, and the least blue shift has been observed in 450 °C annealed TiO<sub>2</sub> thin films. From figure 15 (b), the blue shift of absorption spectra of ZnO ALD thin films has been increased with the increase in annealing temperature. “as-deposited,” ZnO ALD thin films has been exhibited least blue shift and highest absorption in comparison to the annealed ZnO ALD thin films.

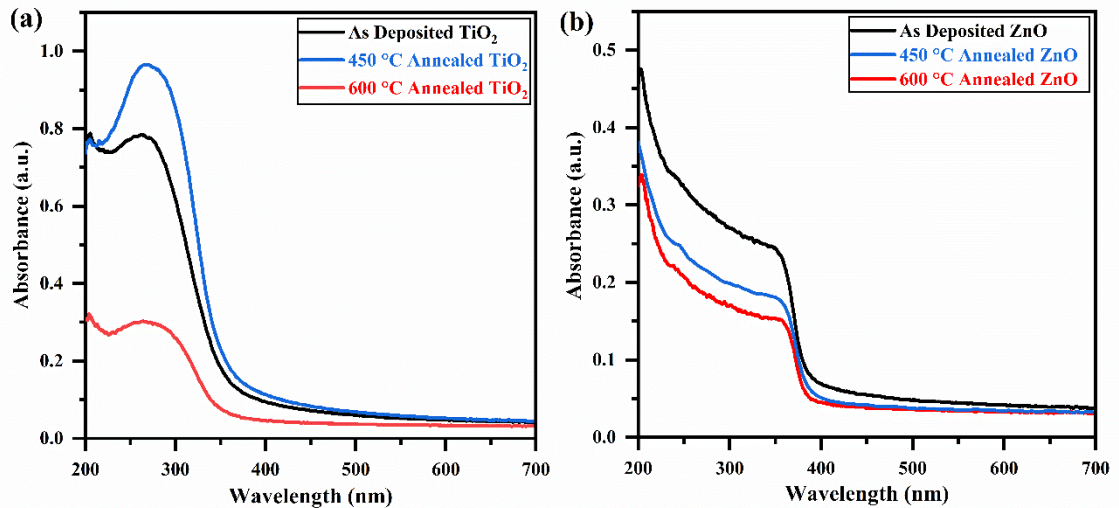


**Figure 15:** UV-Vis Absorption spectra of TiO<sub>2</sub> (a) and ZnO (b) ALD thin films.

Optical bandgap energy of both TiO<sub>2</sub> and ZnO ALD thin films has been estimated from the Tauc plot using Tauc and Devid-Mott relation and optical absorbance data.  $(\alpha h\nu)^{1/n}$  (here,  $n= 2$  for TiO<sub>2</sub> and  $n= \frac{1}{2}$  for ZnO) vs.  $h\nu$  relation was used to construct the Tauc plot. Figure 16 (a) and (b) represents the Tauc plot for both TiO<sub>2</sub> & ZnO and their different annealed ALD thin films. From figure 16 (a), we can see that the optical bandgap energy of TiO<sub>2</sub> ALD thin films was increased with the increase of annealing temperature. The optical bandgap energy of “as-deposited” 450 °C and 600 °C annealed TiO<sub>2</sub> thin

films are 3.08 eV, 3.18 eV, and 3.2 eV, respectively. In literature, the reverse result has been observed. Shi et al. reported that “as-deposited” TiO<sub>2</sub> ALD thin films exhibited the highest bandgap energy and bandgap energy decreased as the increase of annealing temperature up to 600 °C, later bandgap energy again started to increase up to 700 °C and decreased again as the increased in annealing temperature over 700 °C. The lowest bandgap energy had been observed 3.3 eV dropped from 3.4 eV at 900 °C. (Shi et al. 2017). This discrepancy may be originated from the Ti precursor or film thickness variation. In our study, we used Tetrakis (dimethylamido) titanium (TDMAT), where they used Titanium tetraisopropoxide (TTIP). In our study, we used 250 ALD cycles (10 nm), where they used 600 cycles (20 nm) for TiO<sub>2</sub> thin films. In figure 16 (b), the bandgap energy of ZnO ALD and its annealed thin films was increased with the increase of annealing temperature. The optical bandgap energy of “as-deposited” 450 °C and 600 °C annealed ZnO thin films are 3.24 eV, 3.26 eV, and 3.27 eV, respectively. A very little bandgap energy variation is being observed among them. Di Mauro et al. reported that ZnO ALD thin film deposited at 80 °C had bandgap energy was 3.3 eV (Di Mauro et al. 2016). The ZnO thin films synthesized by other thin-film methods such as sputtering and chemical precipitation method had been found that the bandgap energy of ZnO thin films decreased as the increased in annealing temperature (Goswami et al. 2018, Y. Kim et al. 2010). However, Cao et al. reported that the bandgap of ZnO ALD thin films remained in 3.28 eV at annealed between 400 °C to 900 °C (Cao et al. 2015).

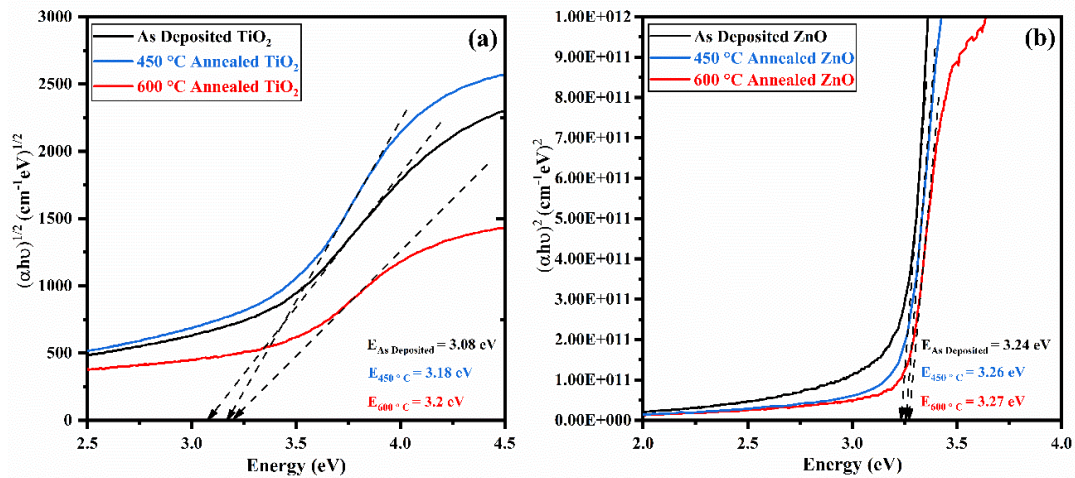


**Figure 16:** Tauc plot of TiO<sub>2</sub> (a) and ZnO (b) ALD thin films.

#### **4.6 Photocatalytic Activity Test of ALD Thin Films**

The TiO<sub>2</sub> and ZnO ALD deposited glass fabrics were employed to evaluate the photocatalytic activities of ALD thin films. The glass fabrics are contained high surface area because of their cylindrical structure of glass fibers. The photocatalytic reaction is pretty responsive to the photocatalyst surface and surface area. The photoreactions have been initiated by absorbing photons from the light sources with energy equal or higher to the bandgap of the catalysts and producing electron-hole pairs from the surface of the catalysts. The electrons generated from the catalyst are reacted with MB and degrade it into CO<sub>2</sub> and H<sub>2</sub>O. The mechanism of the photocatalytic reaction has been discussed in the introduction part.

Figure 17 illustrates the photocatalytic activities of TiO<sub>2</sub> and ZnO ALD thin films under a dark medium. Figure 17 (a) and (b) represents the photocatalytic activities of TiO<sub>2</sub> and ZnO ALD thin films under dark medium, respectively. In Fig 17, it is clearly seen that there is no photocatalytic activities of them either as-deposited TiO<sub>2</sub> and ZnO or their annealed ALD thin films under dark medium. It is evident that the photocatalysts are inactivated without light sources.

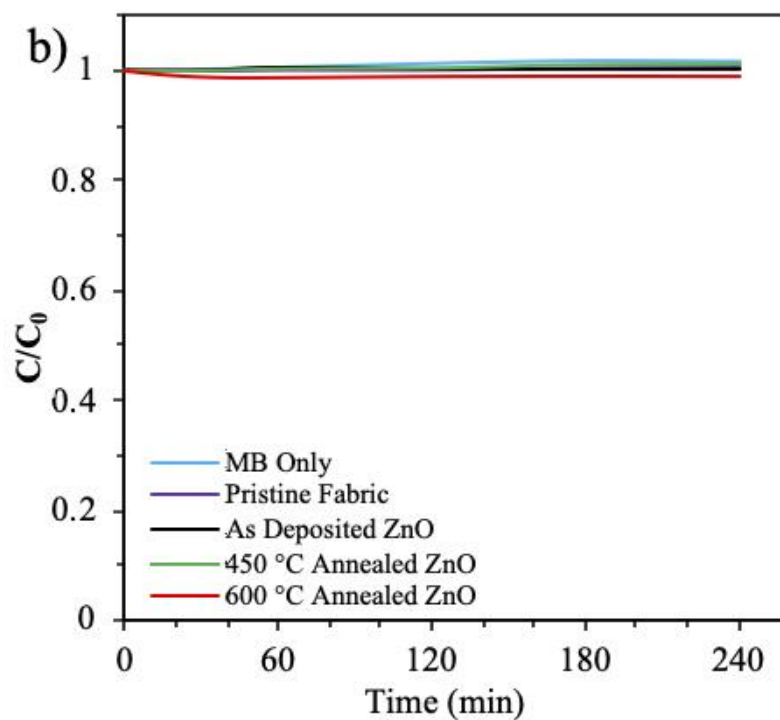
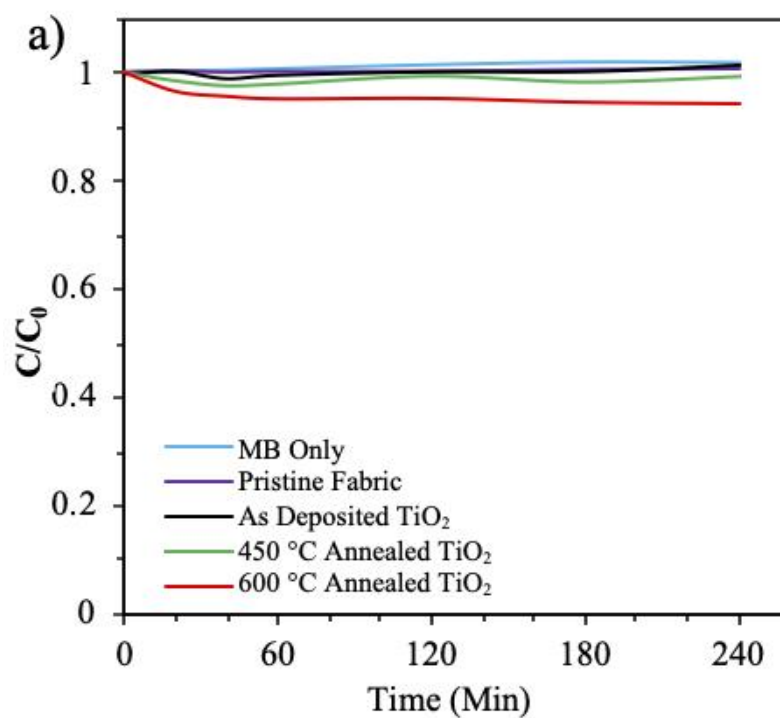


**Figure 17:** Photocatalytic Activities of TiO<sub>2</sub> (a) and ZnO (b) ALD Thin Films Under Dark Medium.

The photocatalytic activities of TiO<sub>2</sub> and ZnO ALD thin films under solar simulator have been demonstrated in Figures 18 (a) and (b), respectively. From figure 18 (a), it is clearly seen that “as-deposited” TiO<sub>2</sub> shows the same photodegradation efficiency as the “MB solution” and pristine fabrics. The results imply that the “as-deposited” TiO<sub>2</sub> ALD thin films is amorphous. In literature, it is well reported that the TiO<sub>2</sub> ALD thin grown at 190 °C or below it, was amorphous (Lee et al. 2013) (Aarik et al. 1995). From the XRD pattern of “as-deposited” TiO<sub>2</sub> ALD thin films also evident that the “as-deposited” TiO<sub>2</sub> ALD film is amorphous. FESEM image of “as-deposited” TiO<sub>2</sub> was depicted the amorphous phase of TiO<sub>2</sub>. In literature, it is also reported the amorphous TiO<sub>2</sub> films did not have or show very little photocatalytic activities under solar energy (Ohtani et al. 1997). Figure 18 (a) also illustrated that the annealed TiO<sub>2</sub> ALD thin films had shown a significant MB photodegradation efficiency in comparison to “as-deposited TiO<sub>2</sub>” thin films. The 450°C annealed TiO<sub>2</sub> thin films have been exhibited higher photocatalytic activities in comparison to the TiO<sub>2</sub> film annealed at 600°C. It has been shown up to 70% of photodegradation efficiency of MB where the 600°C annealed TiO<sub>2</sub> thin films have been produced only 60 % photodegradation efficiency attributing that the presence of anatase form of TiO<sub>2</sub> in 450°C annealed thin films which were transformed from the amorphous phase to crystal anatase at time of annealing process (Li et al. 2009). In XRD results of 450 °C annealed TiO<sub>2</sub> it is also found that 450 °C annealed TiO<sub>2</sub> was anatase. In literature, various reports also articulated that the anatase TiO<sub>2</sub> phase had been exhibited the highest photocatalytic activity than any other phase of TiO<sub>2</sub> (Luttrell et al. 2015). The FESEM images of 450 °C and 600 °C was indicated the crystal grain of TiO<sub>2</sub> thin films; although the grain size was very small so it is difficult to come to any conclusion. The decrease of photocatalytic activity of 600 °C annealed TiO<sub>2</sub> thin film may be originated from the partial phase transformation of the anatase to rutile structure as several reports also have been stated that the rutile structure has less photocatalytic activities than the anatase form of TiO<sub>2</sub> thin films (Li et al. 2009). From the XRD pattern of 450 °C annealed TiO<sub>2</sub>, characteristic anatase peak was observed, and besides, we observed both anatase and rutile sharp peak in XRD pattern at 600 °C annealed TiO<sub>2</sub>, which is justified that the phase transformation had occurred at 600 °C. From tauc plot, we have estimated the bandgap energy of 450 °C and 600 °C annealed TiO<sub>2</sub>, which are 3.18 eV and 3.2 eV, respectively. Here we also find that 450 °C has low bandgap energy than 600 °C annealed

TiO<sub>2</sub>. This may be another reason to show the highest photocatalytic activities by 450 °C annealed TiO<sub>2</sub>. Fig 18(b) represents the photocatalytic activities of ZnO ALD thin films. “As deposited ZnO” films have been exhibited the highest photodegradation of MB up to 96.61 % under the four hours of solar simulator irradiation while the photocatalytic activity of ZnO ALD thin films annealed at 450°C and 600°C has been decreased in comparison to “As deposited ZnO” thin films. The 450°C annealed ZnO thin films have been shown 92.66% of MB photodegradation efficiency, where the 600°C annealed ZnO thin films have been produced only 73.48% MB photodegradation efficiency. It is assumed that the high surface area of hexagonal wurtzite crystal ZnO thin films has been well deposited on the glass fibers resulting in higher photocatalytic activities. From the XRD report, we observed that the XRD pattern of “as-deposited” and 450 °C annealed ZnO ALD thin films showed the sharp wurtzite crystal characteristic peak of ZnO where the sharpness and intensity of the peak were decreased at 600 °C annealed ZnO thin films resulting in the decrease of photocatalytic activities of it. From XPS analysis, we observed that the oxygen vacancy was found at both “as-deposited” and 450 °C annealed ZnO thin films but not found in 600 °C annealed ZnO. In literature, it is reported that the carrier concentration was increased as the concentration of oxygen vacancy  $V_o$  was increased too in the ZnO thin films (Jiang et al. 2017, Y. H. Wang et al. 2016). It is well known that an increase in carrier concentration means an increase in photocatalytic activities (Ben Ameer et al. 2018). From Tauc plot of ZnO ALD thin films, we are observed that “as-deposited” ZnO ALD thin has the lowest bandgap energy that is 3.24 eV, where 450 °C and 600 °C annealed ZnO thin films 3.26 eV and 3.27 eV respectively. It is well known that higher bandgap energy may lead to a decrease in the photocatalytic activities of ZnO thin films (Ben Ameer et al. 2018).

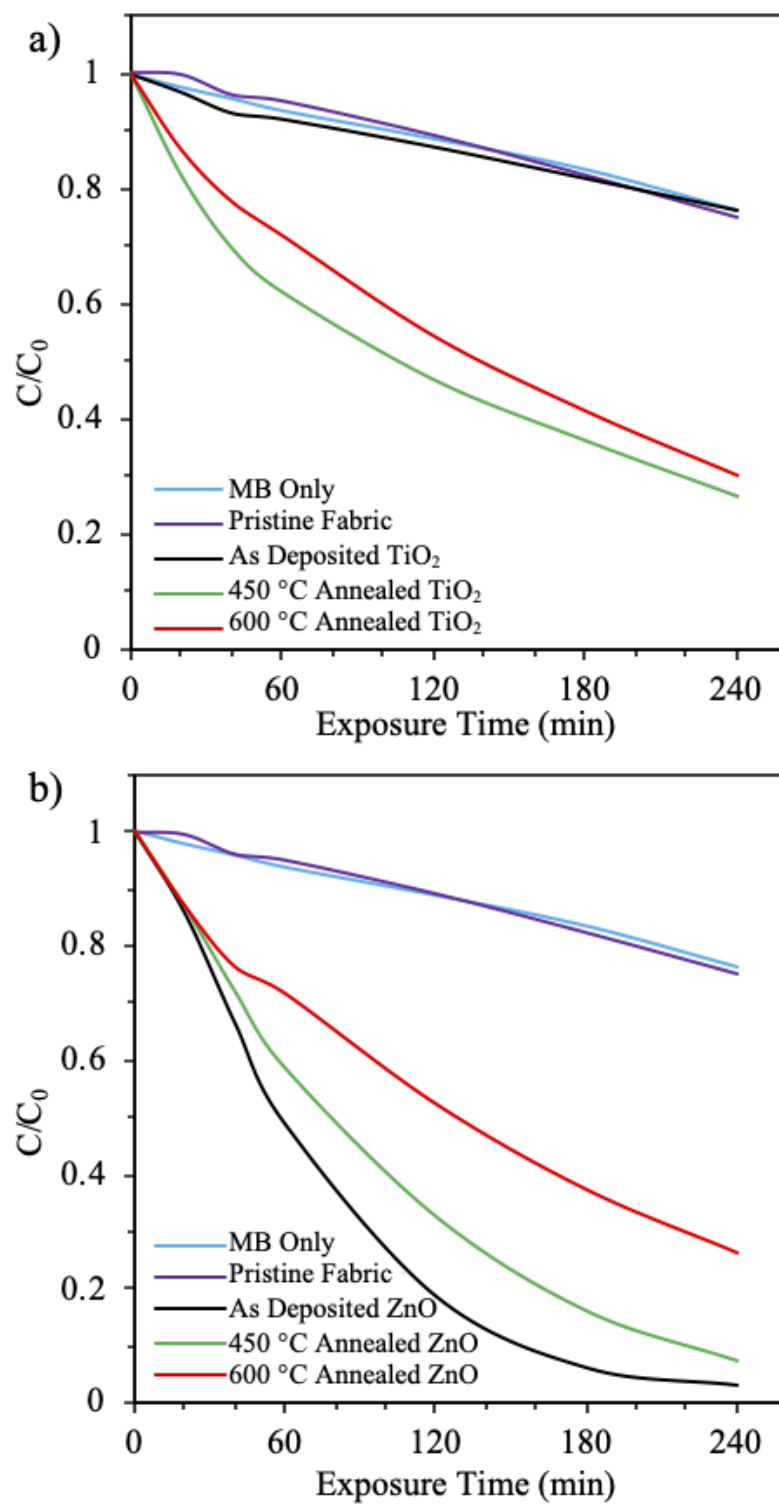


**Figure 18:** Photocatalytic Activities Test of TiO<sub>2</sub> (a) and ZnO (b) ALD thin films under Solar Simulator.

Figure 19 represents the photocatalytic activities of TiO<sub>2</sub> and ZnO ALD thin films under the UV lamp. Figure 19 (a) and (b) represents the photocatalytic activities of TiO<sub>2</sub> and ZnO, respectively. From figure 19 (a), it can be clearly seen that “as-deposited” TiO<sub>2</sub> is not exhibited any photodegradation efficiency under a UV lamp similar to figure 18(a). It also can be seen that the TiO<sub>2</sub> thin films annealed at 450 °C and 600 °C have been shown the same photodegradation efficiency up to 58%. It is clearly observed that the annealed TiO<sub>2</sub> thin films under the solar simulator have been exhibited better photodegradation efficiency than the photodegradation efficiency under the UV lamp. In both light sources, 450 °C annealed TiO<sub>2</sub> has been shown to a better photodegradation efficiency. In fig 19(b), it can be observed that the photodegradation efficiency of ZnO thin films under UV lamp is pretty similar to the photo degradation efficiency under solar simulator. “As deposited ZnO” thin films have been exhibited the highest photodegradation efficiency up to 97%. The photodegradation efficiency of 450 °C and 600 °C annealed ZnO thin films have been dropped to 85% and 64%, respectively.

In conclusion it is found that, the 450 °C annealed TiO<sub>2</sub> among TiO<sub>2</sub>, and “as-deposited” ZnO both TiO<sub>2</sub> and ZnO ALD thin films have been exhibited the highest photocatalytic activities under both solar simulator and UV lamp.

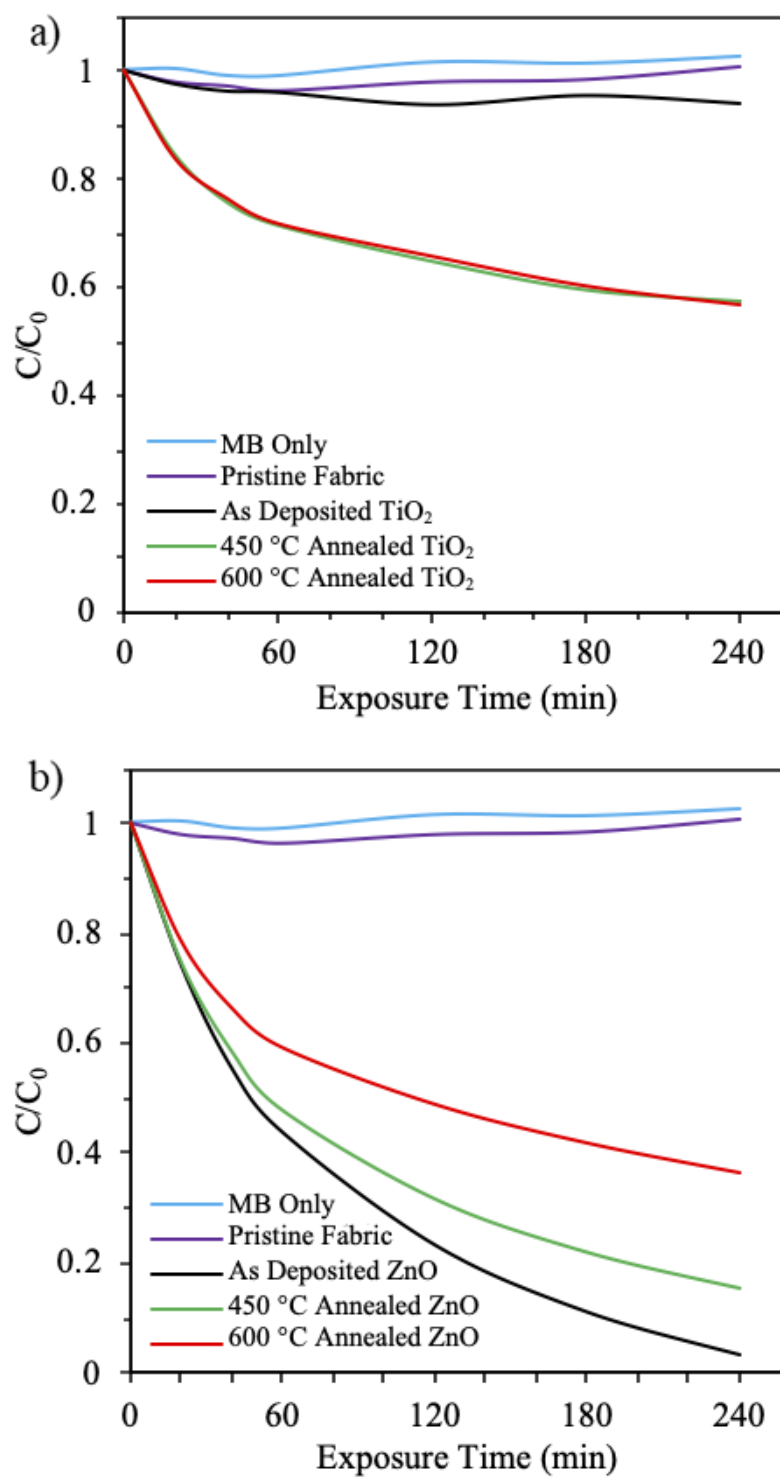


**Figure 19:** Photocatalytic Activities Test of TiO<sub>2</sub> (a) and ZnO (b) ALD thin films under UV lamp.

## 5. CONCLUSION

TiO<sub>2</sub> and ZnO photocatalyst thin films were deposited on glass fabrics by atomic layer deposition (ALD). Approximately 10 nm of a thickness of photocatalyst was deposited on glass fabric. Deposited thin films were annealed at 450 °C and 600 °C for 2 hours in an electric furnace. Methylene blue was used as an organic wastewater source. FESEM, AFM, XPS, XRD, and UV-Vis spectrophotometer were used deeply to investigate the ALD thin films. FESEM report was confirmed a homogenous and uniform coating of ALD thin films. The morphology of the thin films was also investigated by FESEM. 3-D morphology and rms roughness of the thin films was analyzed by AFM. XPS analysis was confirmed the presence TiO<sub>2</sub> and ZnO ALD thin films on glass fabrics. The crystal structure of the thin films was determined by XRD, and optical properties were analyzed by UV-Vis spectrophotometer. Photocatalytic activity of ALD thin films was carried out under dark medium, solar simulator, and UV lamp. No MB degradation was observed under a dark medium. Among the “as-deposited” TiO<sub>2</sub>, 450 °C and 600 °C annealed TiO<sub>2</sub> ALD thin films, 450 °C annealed TiO<sub>2</sub> was showed the highest MB degradation efficiency on four hours of irradiation under both solar simulator and UV lamp. 450 °C annealed TiO<sub>2</sub> was transformed in anatase phase from amorphous was confirmed by XRD pattern. The bandgap energy of 450 °C annealed TiO<sub>2</sub> thin films was lower than 600 °C annealed TiO<sub>2</sub> thin films. Transformed into anatase phase and low bandgap energy lead to 450 °C annealed TiO<sub>2</sub> ALD thin films to show the highest photocatalytic activities. “As deposited” ZnO was showed the highest MB degradation both as TiO<sub>2</sub> and ZnO ALD thin films. It had shown up to 96.6% and 97% MB degradation on four hours of irradiation under solar simulator and UV lamp, respectively. Hexagonal wurtzite crystal structure, oxygen vacancy, and low bandgap energy of “as-deposited” ZnO ALD thin films may lead to show highest MB photodegradation efficiency. The high surface area of glass fiber may have a significant impact on photocatalytic activities of both TiO<sub>2</sub> and ZnO ALD thin films.

## REFERENCES

- Aarik, J., Aidla, A., Uustare, T., Sammelselg, V. 1995.** Morphology and structure of TiO<sub>2</sub> thin films grown by atomic layer deposition. *Journal of Crystal Growth*, 148(3): 268–275. [https://doi.org/10.1016/0022-0248\(94\)00874](https://doi.org/10.1016/0022-0248(94)00874)
- Abe, R., Higashi, M., Sayama, K., Abe, Y., Sugihara, H. 2006.** Photocatalytic Activity of R<sub>3</sub>MO<sub>7</sub> and R<sub>2</sub>Ti<sub>2</sub>O<sub>7</sub> (R: Y, Gd, La; M: Nb, Ta) for Water Splitting into H<sub>2</sub> and O<sub>2</sub>. *ChemInform*, 37(16): 2219–2226. <https://doi.org/10.1002/chin.200616023>
- Ahn, H. J., Kwak, M. J., Lee, J. S., Yoon, K. Y., Jang, J. H. 2014.** Nanoporous hematite structures to overcome short diffusion lengths in water splitting. *Journal of Materials Chemistry A*, 2(47): 19999–20003. <https://doi.org/10.1039/c4ta04890c>
- Akpan, U. G., Hameed, B. H. 2009.** Parameters affecting the photocatalytic degradation of dyes using TiO<sub>2</sub>-based photocatalysts: A review. *Journal of Hazardous Materials*, 170(2–3): 520–529. <https://doi.org/10.1016/j.jhazmat.2009.05.039>
- Al-Hamdi, A. M., Rinner, U., Sillanpää, M. 2017.** Tin dioxide as a photocatalyst for water treatment: A review. *Process Safety and Environmental Protection*, 107: 190–205. <https://doi.org/10.1016/j.psep.2017.01.022>
- Aslam, M., Qamar, M. T., Soomro, M. T., Ismail, I. M. I., Salah, N., Almeelbi, T., Gondal, M. A., Hameed, A. 2016.** The effect of sunlight induced surface defects on the photocatalytic activity of nanosized CeO<sub>2</sub> for the degradation of phenol and its derivatives. *Applied Catalysis B: Environmental*, 180: 391–402. <https://doi.org/10.1016/j.apcatb.2015.06.050>
- Babuponnusami, A., Muthukumar, K. 2014.** A review on Fenton and improvements to the Fenton process for wastewater treatment. *Journal of Environmental Chemical Engineering*, 2(1): 557–572. <https://doi.org/10.1016/j.jece.2013.10.011>
- Barajas-Ledesma, E., García-Benjume, M. L., Espitia-Cabrera, I., Bravo-Patiño, A., Espinoza-Beltrán, F. J., Mostaghimi, J., Contreras-García, M. E. 2010.** Photocatalytic activity of Al<sub>2</sub>O<sub>3</sub>-doped TiO<sub>2</sub> thin films activated with visible light on the bacteria *Escherichia coli*. *Materials Science and Engineering B: Solid-State Materials for Advanced Technology*, 174(1–3): 74–79. <https://doi.org/10.1016/j.mseb.2010.03.024>
- Ben Ameer, S., Bel hadjltaief, H., Barhoumi, A., Duponchel, B., Leroy, G., Amlouk, M., Guermazi, H. 2018.** Physical investigations and photocatalytic activities on ZnO and SnO<sub>2</sub> thin films deposited on flexible polymer substrate. *Vacuum*, 155: 546–552. <https://doi.org/10.1016/j.vacuum.2018.05.051>

**Bhattacharjee, A., Ahmaruzzaman, M. 2015.** Photocatalytic-degradation and reduction of organic compounds using SnO<sub>2</sub> quantum dots (via a green route) under direct sunlight. *RSC Advances*, 5(81): 66122–66133. <https://doi.org/10.1039/c5ra07578e>

**Borges, M. E., Sierra, M., Cuevas, E., García, R. D., Esparza, P. 2016.** Photocatalysis with solar energy : Sunlight-responsive photocatalyst based on TiO<sub>2</sub> loaded on a natural material for wastewater treatment. *Solar Energy*, 135: 527–535. <https://doi.org/10.1016/j.solener.2016.06.022>

**Boukos, N., Chandrinou, C., Travlos, A. 2012.** Zinc vacancies and interstitials in ZnO nanorods. *Thin Solid Films*, 520(14): 4654–4657. <https://doi.org/10.1016/j.tsf.2011.10.138>

**Byun, D., Jin, Y., Kim, B., Kee Lee, J., Park, D. 2000.** Photocatalytic TiO<sub>2</sub> deposition by chemical vapor deposition. *Journal of Hazardous Materials*, 73(2): 199–206. [https://doi.org/10.1016/S0304-3894\(99\)00179-X](https://doi.org/10.1016/S0304-3894(99)00179-X)

**Cao, Y. Q., Chen, J., Zhou, H., Zhu, L., Li, X., Cao, Z. Y., Wu, D., Li, A. D. 2015.** Photocatalytic activity and photocorrosion of atomic layer deposited ZnO ultrathin films for the degradation of methylene blue. *Nanotechnology*, 26(2). <https://doi.org/10.1088/0957-4484/26/2/024002>

**Chen, F., Zhou, R., Yang, L., Shi, M., Wu, G., Wang, M., Chen, H. 2008.** One-step fabrication of CdS nanorod arrays via solution chemistry. *Journal of Physical Chemistry C*, 112(35):13457–13462. <https://doi.org/10.1021/jp802745b>

**Chen, L. X., Liu, T., Thurnauer, M. C., Csencsits, R., Rajh, T. 2002.** Fe<sub>2</sub>O<sub>3</sub> nanoparticle structures investigated by X-ray absorption near-edge structure, surface modifications, and model calculations. *Journal of Physical Chemistry B*, 106(34): 8539–8546. <https://doi.org/10.1021/jp025544x>

**Cheng, L., Xiang, Q., Liao, Y., Zhang, H. 2018.** CdS-Based photocatalysts. *Energy and Environmental Science*, 11(6): 1362–1391. <https://doi.org/10.1039/c7ee03640j>

**Chollom, M. N., Rathilal, S., Pillay, V. L., Alfa, D. 2015.** The applicability of nanofiltration for the treatment and reuse of textile reactive dye effluent. *Water SA*, 41(3): 398–405. <https://doi.org/10.4314/wsa.v41i3.12>

**Chong, M. N., Jin, B., Chow, C. W. K., Saint, C. 2010.** Recent developments in photocatalytic water treatment technology: A review. *Water Research*, 44(10): 2997–3027. <https://doi.org/10.1016/j.watres.2010.02.039>

**Dang, V. S., Parala, H., Kim, J. H., Xu, K., Srinivasan, N. B., Edengeiser, E., Havenith, M., Wieck, A. D., De Los Arcos, T., Fischer, R. A., Devi, A. 2014.** Electrical and optical properties of TiO<sub>2</sub> thin films prepared by plasma-enhanced atomic layer deposition. *Physica Status Solidi (A) Applications and Materials Science*, 211(2): 416–424. <https://doi.org/10.1002/pssa.201330115>

**Dasgupta, N. P., Meng, X., Elam, J. W., Martinson, A. B. F. 2015.** Atomic layer deposition of metal sulfide materials. *Accounts of Chemical Research*, 48(2): 341–348. <https://doi.org/10.1021/ar500360d>

**Di Mauro, A., Cantarella, M., Nicotra, G., Privitera, V., Impellizzeri, G. 2016.** Low temperature atomic layer deposition of ZnO: Applications in photocatalysis. *Applied Catalysis B: Environmental*, 196: 68–76. <https://doi.org/10.1016/j.apcatb.2016.05.015>

**Fang, D., Luo, Z., Huang, K., Lagoudas, D. C. 2011.** Effect of heat treatment on morphology, crystalline structure and photocatalysis properties of TiO<sub>2</sub> nanotubes on Ti substrate and freestanding membrane. *Applied Surface Science*, 257(15): 6451–6461. <https://doi.org/10.1016/j.apsusc.2011.02.037>

**Fenoll, J., Ruiz, E., Hellín, P., Flores, P., Navarro, S. 2011.** Heterogeneous photocatalytic oxidation of cyprodinil and fludioxonil in leaching water under solar irradiation. *Chemosphere*, 85(8): 1262–1268. <https://doi.org/10.1016/j.chemosphere.2011.07.022>

**Frank, S. N., Bard, A. J. 1977.** Heterogeneous Photocatalytic Oxidation of Cyanide Ion in Aqueous Solutions at TiO<sub>2</sub> Powder. *Journal of the American Chemical Society*, 99(1): 303–304. <https://doi.org/10.1021/ja00443a081>

**Fujishima, A., and Honda, K. 1972.** MOLECULAR Electrochemical Photolysis of Water at a Semiconductor Electrode One and Two-dimensional Structure of Alpha-Helix and Beta-Sheet Forms of Poly ( L-Alanine ) shown by Specific Heat Measurements at Low Temperatures ( 1 . 5-20 K ). *Nature*, 238: 37–38.

**Fujishima, A., Rao, T. N., Tryk, D. A. 2000.** Titanium dioxide photocatalysis. *Journal of Photochemistry and Photobiology C: Photochemistry Reviews*, 1(1): 1–21.

**Fujishima, A., Zhang, X., Tryk, D. A. 2008.** TiO<sub>2</sub> photocatalysis and related surface phenomena. *Surface Science Reports*, 63(12): 515–582. <https://doi.org/10.1016/j.surfrep.2008.10.001>

**Furlan, K. P., Krekeler, T., Ritter, M., Blick, R., Schneider, G. A., Nielsch, K., Zierold, R., Janßen, R. 2017.** Low-Temperature Mullite Formation in Ternary Oxide Coatings Deposited by ALD for High-Temperature Applications. *Advanced Materials Interfaces*, 4(23): 1–8. <https://doi.org/10.1002/admi.201700912>

**Garzella, C., Comini, E., Tempesti, E., Frigeri, C., Sberveglieri, G. 2000.** TiO<sub>2</sub> thin films by a novel sol-gel processing for gas sensor applications. *Sensors and Actuators, B: Chemical*, 68(1): 189–196. [https://doi.org/10.1016/S0925-4005\(00\)00428-7](https://doi.org/10.1016/S0925-4005(00)00428-7)

**Gebhard, M., Mitschker, F., Wiesing, M., Giner, I., Torun, B., De Los Arcos,**

**T., Awakowicz, P., Grundmeier, G., Devi, A. 2016.** An efficient PE-ALD process for TiO<sub>2</sub> thin films employing a new Ti-precursor. *Journal of Materials Chemistry C*, 4(5): 1057–1065. <https://doi.org/10.1039/c5tc03385c>

**Gharoy Ahangar, E., Abbaspour-Fard, M. H., Shahtahmassebi, N., Khojastehpour, M., Maddahi, P. 2015.** Preparation and Characterization of PVA/ZnO Nanocomposite. *Journal of Food Processing and Preservation*, 39(6): 1442–1451. <https://doi.org/10.1111/jfpp.12363>

**Gong, J., Meng, F., Yang, X., Fan, Z., Li, H. 2016.** Controlled hydrothermal synthesis of triangular CeO<sub>2</sub> nanosheets and their formation mechanism and optical properties. *Journal of Alloys and Compounds*, 689: 606–616. <https://doi.org/10.1016/j.jallcom.2016.08.030>

**Goodeve, C. F., Kitchener, J. A. 1938.** Photosensitisation by titanium dioxide. *Transactions of the Faraday Society*, 34(570): 570–579. <https://doi.org/10.1039/TF9383400570>

**Goswami, M., Adhikary, N. C., Bhattacharjee, S. 2018.** Effect of annealing temperatures on the structural and optical properties of zinc oxide nanoparticles prepared by chemical precipitation method. *Optik*, 158: 1006–1015. <https://doi.org/10.1016/j.ijleo.2017.12.174>

**Guo, H. C., Ye, E., Li, Z., Han, M. Y., Loh, X. J. 2017.** Recent progress of atomic layer deposition on polymeric materials. *Materials Science and Engineering C*, 70: 1182–1191. <https://doi.org/10.1016/j.msec.2016.01.093>

**Gupta, V. K., Gupta, B., Rastogi, A., Agarwal, S., Nayak, A. 2011.** A comparative investigation on adsorption performances of mesoporous activated carbon prepared from waste rubber tire and activated carbon for a hazardous azo dye-Acid Blue 113. *Journal of Hazardous Materials*, 186(1): 891–901. <https://doi.org/10.1016/j.jhazmat.2010.11.091>

**Hashimoto, K., Irie, H., Fujishima, A. 2005.** TiO<sub>2</sub> photocatalysis: A historical overview and future prospects. *Japanese Journal of Applied Physics, Part 1: Regular Papers and Short Notes and Review Papers*, 44(12): 8269–8285. <https://doi.org/10.1143/JJAP.44.8269>

**Hoek, E. M. V., Tarabara, V. V., Koyuncu, I., Güney, K. 2013.** Membrane-Based Treatment of Textile Industry Wastewaters. *Encyclopedia of Membrane Science and Technology*, 1-12. <https://doi.org/10.1002/9781118522318.emst127>

**Hoffmann, M. R., Martin, S. T., Choi, W., Bahnemann, D. W. 1995.** Environmental Applications of Semiconductor Photocatalysis. *Chemical Reviews*, 95(1): 69–96. <https://doi.org/10.1021/cr00033a004>

**Holkar, C. R., Jadhav, A. J., Pinjari, D. V., Mahamuni, N. M., Pandit, A. B. 2016.** A critical review on textile wastewater treatments: Possible approaches.

Journal of Environmental Management, 182, 351–366.  
<https://doi.org/10.1016/j.jenvman.2016.07.090>

**Hultqvist, A., Edoff, M., Törndahl, T. 2011.** Solar cell efficiency tables (version 40). PROGRESS IN PHOTOVOLTAICS, 20(19): 478–481.  
<https://doi.org/https://doi.org/10.1002/pip.1039>

**Hyde, G. K., McCullen, S. D., Jeon, S., Stewart, S. M., Jeon, H., Lobo, E. G., Parsons, G. N. 2009.** Atomic layer deposition and biocompatibility of titanium nitride nano-coatings on cellulose fiber substrates. Biomedical Materials, 4(2).  
<https://doi.org/10.1088/1748-6041/4/2/025001>

**Hyde, G. Kevin, Park, K. J., Stewart, S. M., Hinstroza, J. P., Parsons, G. N. 2007.** Atomic layer deposition of conformal inorganic nanoscale coatings on three-dimensional natural fiber systems: Effect of surface topology on film growth characteristics. Langmuir, 23(19): 9844–9849. <https://doi.org/10.1021/la701449t>

**Iqbal, J., Jilani, A., Ziaul Hassan, P. M., Rafique, S., Jafer, R., Alghamdi, A. A. 2016.** ALD grown nanostructured ZnO thin films: Effect of substrate temperature on thickness and energy band gap. Journal of King Saud University - Science, 28(4): 347–354. <https://doi.org/10.1016/j.jksus.2016.03.001>

**Jang, E. S., Won, J. H., Hwang, S. J., Choy, J. H. 2006.** Fine tuning of the face orientation of ZnO crystals to optimize their photocatalytic activity. Advanced Materials, 18(24): 3309–3312. <https://doi.org/10.1002/adma.200601455>

**Jeong, B., Kim, D. H., Park, E. J., Jeong, M. G., Kim, K. D., Seo, H. O., Kim, Y. D., Uhm, S. 2014.** ZnO shell on mesoporous silica by atomic layer deposition: Removal of organic dye in water by an adsorbent and its photocatalytic regeneration. Applied Surface Science, 307, 468–474.  
<https://doi.org/10.1016/j.apsusc.2014.04.060>

**Jiang, L., Li, J., Huang, K., Li, S., Wang, Q., Sun, Z., Mei, T., Wang, J., Zhang, L., Wang, N., Wang, X. 2017.** Low-Temperature and Solution-Processable Zinc Oxide Transistors for Transparent Electronics. ACS Omega, 2(12): 8990–8996.  
<https://doi.org/10.1021/acsomega.7b01420>

**Jnido, G., Ohms, G., Viöl, W. 2019.** Deposition of TiO<sub>2</sub> thin films on wood substrate by an air atmospheric pressure plasma jet. Coatings, 9(7): 441.  
<https://doi.org/10.3390/coatings9070441>

**Johnson, R. W., Hultqvist, A., Bent, S. F. 2014.** A brief review of atomic layer deposition: From fundamentals to applications. Materials Today, 17(5): 236–246.  
<https://doi.org/10.1016/j.mattod.2014.04.026>

**Jur, J. S., Sweet, W. J., Oldham, C. J., Parsons, G. N. 2011.** Atomic layer deposition of conductive coatings on cotton, paper, and synthetic fibers: Conductivity analysis and functional chemical sensing using “all-fiber” capacitors.

Advanced Functional Materials, 21(11): 1993–2002.  
<https://doi.org/10.1002/adfm.201001756>

**Kang, S., Mauchauffé, R., You, Y. S., Moon, S. Y. 2018.** Insights into the Role of Plasma in Atmospheric Pressure Chemical Vapor Deposition of Titanium Dioxide Thin Films. *Scientific Reports*, 8(1): 1–14. <https://doi.org/10.1038/s41598-018-35154-4>

**Kangwansupamonkon, W., Lauruengtana, V. 2009.** Antibacterial effect of apatite-coated titanium dioxide for textiles applications. *Nanomedicine: Nanotechnology, Biology, and Medicine*, 5(2): 240–249. <https://doi.org/10.1016/j.nano.2008.09.004>

**Kavan, L., Grätzel, M., Gilbert, S. E., Klemenz, C., Scheel, H. J. 1996.** Electrochemical and photoelectrochemical investigation of single-crystal anatase. *Journal of the American Chemical Society*, 118(28): 6716–6723. <https://doi.org/10.1021/ja9541721>

**Kawai, T., Sakata, T. 1980.** Conversion of carbohydrate into hydrogen fuel by a photocatalytic process. *Nature*, 286(5772): 474–476. <https://doi.org/10.1038/286474a0>

**Kayaci, F., Ozgit-Akgun, C., Biyikli, N., Uyar, T. 2013.** Surface-decorated ZnO nanoparticles and ZnO nanocoating on electrospun polymeric nanofibers by atomic layer deposition for flexible photocatalytic nanofibrous membranes. *RSC Advances*, 3(19): 6817–6820. <https://doi.org/10.1039/c3ra40359a>

**Khan, M. M., Adil, S. F., Al-Mayouf, A. 2015.** Metal oxides as photocatalysts. *Journal of Saudi Chemical Society*, 19(5): 462–464. <https://doi.org/10.1016/j.jscs.2015.04.003>

**Khan, M. M., Pradhan, D., Sohn, Y. 2017.** Springer Series on Polymer and Composite Materials Nanocomposites for Visible Light-induced Photocatalysis. *Nanocomposites for Visible Light-induced Photocatalysis*, 19–40. <https://doi.org/10.1007/978-3-319-62446-4>

**Kim, H. 2003.** Atomic layer deposition of metal and nitride thin films: Current research efforts and applications for semiconductor device processing. *Journal of Vacuum Science and Technology B: Microelectronics and Nanometer Structures*, 21(6): 2231–2261. <https://doi.org/10.1116/1.1622676>

**Kim, J., Hong, H., Ghosh, S., Oh, K. Y., Lee, C. 2003.** Physical properties of highly conformal TiN thin films grown by atomic layer deposition. *Japanese Journal of Applied Physics, Part 1: Regular Papers and Short Notes and Review Papers*, 42(3): 1375–1379. <https://doi.org/10.1143/jjap.42.1375>

**Kim, S., Park, H., Choi, W. 2004.** Comparative study of homogeneous and heterogeneous photocatalytic redox reactions: PW12O40<sup>3-</sup> vs TiO<sub>2</sub>. *Journal of*

Physical Chemistry B, 108(20): 6402–6411. <https://doi.org/10.1021/jp049789g>  
**Kim, Y., Lee, W., Jung, D. R., Kim, J., Nam, S., Kim, H., Park, B. 2010.** Optical and electronic properties of post-annealed ZnO:Al thin films. *Applied Physics Letters*, 96(17): 1–4. <https://doi.org/10.1063/1.3419859>

**Espitia, P. J. P., Soares, N. D. F. F., dos Reis Coimbra, J. S., de Andrade, N. J., Cruz, R. S., & Medeiros, E. A. A. (2012).** Zinc oxide nanoparticles: synthesis, antimicrobial activity and food packaging applications. *Food and bioprocess technology*, 5(5), 1447-1464.

**Konstantinou, I. K., Albanis, T. A. 2004.** TiO<sub>2</sub>-assisted photocatalytic degradation of azo dyes in aqueous solution: Kinetic and mechanistic investigations: A review. *Applied Catalysis B: Environmental*, 49(1): 1–14. <https://doi.org/10.1016/j.apcatb.2003.11.010>

**Kosola, A., Putkonen, M., Johansson, L. S., Niinistö, L. 2003.** Effect of annealing in processing of strontium titanate thin films by ALD. *Applied Surface Science*, 211(1–4): 102–112. [https://doi.org/10.1016/S0169-4332\(03\)00175-2](https://doi.org/10.1016/S0169-4332(03)00175-2)

**Ku-Herrera, J. J., Avilés, F., Nistal, A., Cauich-Rodríguez, J. V., Rubio, F., Rubio, J., Bartolo-Pérez, P. 2015.** Interactions between the glass fiber coating and oxidized carbon nanotubes. *Applied Surface Science*, 330: 383–392. <https://doi.org/10.1016/j.apsusc.2015.01.025>

**Kumar, N., Joo, M., Kim, K., Ook, H., Kim, D., Dok, Y., Chan, D., Hwan, K. 2011.** *Journal of Molecular Catalysis A : Chemical Adsorption and photocatalytic degradation of methylene blue over TiO<sub>2</sub> films on carbon fiber prepared by atomic layer deposition.* “*Journal of Molecular Catalysis. A, Chemical*,” 337(1–2): 33–38. <https://doi.org/10.1016/j.molcata.2011.01.010>

**Kumari, S., Singh, A. P., Tripathi, C., Chauhan, D., Dass, S., Shrivastav, R., Gupta, V., Sreenivas, K., Satsangi, V. R. 2007.** Enhanced photoelectrochemical response of Zn-dotted hematite. *International Journal of Photoenergy*, 2007: 6. <https://doi.org/10.1155/2007/87467>

**Lee, J., Lee, S. J., Han, W. B., Jeon, H., Park, J., Jang, W., Yoon, C. S., Jeon, H. 2013.** Deposition temperature dependence of titanium oxide thin films grown by remote-plasma atomic layer deposition. *Physica Status Solidi (A) Applications and Materials Science*, 210(2): 276–284. <https://doi.org/10.1002/pssa.201228671>

**Leow, W. R., Ng, W. K. H., Peng, T., Liu, X., Li, B., Shi, W., Lum, Y., Wang, X., Lang, X., Li, S., Mathews, N., Ager, J. W., Sum, T. C., Hirao, H., Chen, X. 2017.** Al<sub>2</sub>O<sub>3</sub> surface complexation for photocatalytic organic transformations. *Journal of the American Chemical Society*, 139(1): 269–276. <https://doi.org/10.1021/jacs.6b09934>

**Li, G., Liu, Z. Q., Lu, J., Wang, L., Zhang, Z. 2009.** Effect of calcination temperature on the morphology and surface properties of TiO<sub>2</sub> nanotube arrays.

Applied Surface Science, 255(16): 7323–7328.  
<https://doi.org/10.1016/j.apsusc.2009.03.097>

**Liang, C. Z., Sun, S. P., Li, F. Y., Ong, Y. K., Chung, T. S. 2014.** Treatment of highly concentrated wastewater containing multiple synthetic dyes by a combined process of coagulation/flocculation and nanofiltration. *Journal of Membrane Science*, 469: 306–315. <https://doi.org/10.1016/j.memsci.2014.06.057>

**Liu, G., Yang, H. G., Wang, X., Cheng, L., Lu, H., Wang, L., Lu, G. Q., Cheng, H. M. 2009.** Enhanced photoactivity of oxygen-deficient anatase TiO<sub>2</sub> sheets with dominant {001} facets. *Journal of Physical Chemistry C*, 113(52): 21784–21788. <https://doi.org/10.1021/jp907749r>

**Luttrell, T., Halpegamage, S., Tao, J., Kramer, A., Sutter, E., Batzill, M. 2015.** Why is anatase a better photocatalyst than rutile? - Model studies on epitaxial TiO<sub>2</sub> films. *Scientific Reports*, 4: 1–8. <https://doi.org/10.1038/srep04043>

**M, H. T. E. D. C., Wu, N., Zhu, F. 2000.** A KINETIC MODEL FOR PHOTOCATALYTIC DEGRADATION OF ORGANIC CONTAMINANTS IN A THIN-FILM TiO<sub>2</sub> CATALYST. , 34(2): 407–416.

**Ma, R., Zhang, S., Wen, T., Gu, P., Li, L., Zhao, G., Niu, F., Huang, Q., Tang, Z., Wang, X. 2019.** A critical review on visible-light-response CeO<sub>2</sub>-based photocatalysts with enhanced photooxidation of organic pollutants. *Catalysis Today*, 335: 20–30. <https://doi.org/10.1016/j.cattod.2018.11.016>

**Makula, P., Pacia, M., Macyk, W. 2018.** How To Correctly Determine the Band Gap Energy of Modified Semiconductor Photocatalysts Based on UV-Vis Spectra. *Journal of Physical Chemistry Letters*, 9(23): 6814–6817. <https://doi.org/10.1021/acs.jpcclett.8b02892>

**Matsunaga, T., Tomoda, R., Nakajima, T., Nakamura, N., Komine, T. 1988.** Continuous-sterilization system that uses photoconductor powders. *Applied and environmental microbiology*, 54(6): 1330–1333. <https://doi.org/10.1128/aem.54.6.1330-1333.1988>

**Matthews, R. W. 1987.** Photooxidation of organic impurities in water using thin films of titanium dioxide. *Journal of Physical Chemistry*, 91(12): 3328–3333. <https://doi.org/10.1021/j100296a044>

**Mavukkandy, M. O., McBride, S. A., Warsinger, D. M., Dizge, N., Hasan, S. W., Arafat, H. A. 2020.** Thin film deposition techniques for polymeric membranes – A review. *Journal of Membrane Science*, 610: 118258. <https://doi.org/10.1016/j.memsci.2020.118258>

**Miao, L., Jin, P., Kaneko, K., Terai, A., Nabatova-Gabain, N., Tanemura, S. 2003.** Preparation and characterization of polycrystalline anatase and rutile TiO<sub>2</sub> thin films by rf magnetron sputtering. *Applied Surface Science*, 212–213: 255–263.

[https://doi.org/10.1016/S0169-4332\(03\)00106-5](https://doi.org/10.1016/S0169-4332(03)00106-5)

**Molina-Reyes, J., Romero-Moran, A., Uribe-Vargas, H., Lopez-Ruiz, B., Sanchez-Salas, J. L., Ortega, E., Ponce, A., Morales-Sanchez, A., Lopez-Huerta, F., Zuñiga-Islas, C. 2020.** Study on the photocatalytic activity of titanium dioxide nanostructures: Nanoparticles, nanotubes and ultra-thin films. *Catalysis Today*, 341: 2–12. <https://doi.org/10.1016/j.cattod.2018.05.033>

**Nakata, K., Fujishima, A. 2012.** TiO<sub>2</sub> photocatalysis: Design and applications. *Journal of Photochemistry and Photobiology C: Photochemistry Reviews*, 13(3): 169–189. <https://doi.org/10.1016/j.jphotochemrev.2012.06.001>

**Nasr, M., Viter, R., Eid, C., Habchi, R., Miele, P., Bechelany, M. 2018.** Optical and structural properties of Al<sub>2</sub>O<sub>3</sub> doped ZnO nanotubes prepared by ALD and their photocatalytic application. *Surface and Coatings Technology*, 343: 24–29. <https://doi.org/10.1016/j.surfcoat.2017.11.060>

**Ni, M., Leung, M. K. H., Leung, D. Y. C., Sumathy, K. 2007.** A review and recent developments in photocatalytic water-splitting using TiO<sub>2</sub> for hydrogen production. *Renewable and Sustainable Energy Reviews*, 11(3): 401–425. <https://doi.org/10.1016/j.rser.2005.01.009>

**Ohtani, B., Ogawa, Y., & Nishimoto, S. I. (1997).** Photocatalytic activity of amorphous–anatase mixture of titanium (IV) oxide particles suspended in aqueous solutions. *The Journal of Physical Chemistry B*, 101(19): 3746–3752.

**Ong, C. B., Ng, L. Y., Mohammad, A. W. 2018.** A review of ZnO nanoparticles as solar photocatalysts: Synthesis, mechanisms and applications. *Renewable and Sustainable Energy Reviews*, 81(August 2017): 536–551. <https://doi.org/10.1016/j.rser.2017.08.020>

**Pal, D., Mathur, A., Singh, A., Singhal, J., Sengupta, A., Dutta, S., Zollner, S., Chattopadhyay, S. 2017.** Tunable optical properties in atomic layer deposition grown ZnO thin films. *Journal of Vacuum Science & Technology A: Vacuum, Surfaces, and Films*, 35(1): 01B108. <https://doi.org/10.1116/1.4967296>

**Pore, B. V., Rahtu, A., Leskelä, M., Ritala, M., Sajavaara, T., Keinonen, J. 2004.** Atomic Layer Deposition of Photocatalytic TiO<sub>2</sub> Thin Films From Titanium Tetramethoxide and Water, (3): 143–148. <https://doi.org/10.1002/cvde.200306289>

**Pore, V., Heikkil, M., Ritala, M., Leskela, M., Areva, S. 2006.** Atomic layer deposition of TiO<sub>2</sub>–xN<sub>x</sub> thin films for photocatalytic applications. *Journal of Photochemistry and Photobiology A: Chemistry*, 177(1): 68–75. <https://doi.org/https://doi.org/10.1016/j.jphotochem.2005.05.013>

**Pore, V., Kivel, T. 2008.** Atomic layer deposition of photocatalytic TiO<sub>2</sub> thin films from TiF<sub>4</sub> and H<sub>2</sub>O. *Dalton Transactions*, (45): 6467–6474. <https://doi.org/10.1039/b809953g>

**Potts, S. E., Keuning, W., Langereis, E., Dingemans, G., van de Sanden, M. C. M., Kessels, W. M. M. 2010.** Low Temperature Plasma-Enhanced Atomic Layer Deposition of Metal Oxide Thin Films. *Journal of The Electrochemical Society*, 157(7): 66. <https://doi.org/10.1149/1.3428705>

**Purohit, A., Chander, S., Sharma, A., Nehra, S. P., Dhaka, M. S. 2015.** Impact of low temperature annealing on structural, optical, electrical and morphological properties of ZnO thin films grown by RF sputtering for photovoltaic applications. *Optical Materials*, 49: 51–58. <https://doi.org/10.1016/j.optmat.2015.08.021>

**Qi, K., Cheng, B., Yu, J., Ho, W. 2017.** Review on the improvement of the photocatalytic and antibacterial activities of ZnO. *Journal of Alloys and Compounds*, 727: 792–820. <https://doi.org/10.1016/j.jallcom.2017.08.142>

**Qiu, R., Zhang, D., Mo, Y., Song, L., Brewer, E., Huang, X., Xiong, Y. 2008.** Photocatalytic activity of polymer-modified ZnO under visible light irradiation. *Journal of Hazardous Materials*, 156(1–3): 80–85. <https://doi.org/10.1016/j.jhazmat.2007.11.114>

**Rajeshwar, K., Osugi, M. E., Chanmanee, W., Chenthamarakshan, C. R., Zaroni, M. V. B., Kajitvichyanukul, P., Krishnan-Ayer, R. 2008.** Heterogeneous photocatalytic treatment of organic dyes in air and aqueous media. *Journal of Photochemistry and Photobiology C: Photochemistry Reviews*, 9(4): 171–192. <https://doi.org/10.1016/j.jphotochemrev.2008.09.001>

**Razzaq, A., Sinhamahapatra, A., Kang, T. H., Grimes, C. A., Yu, J. S., In, S. H. 2017.** Efficient solar light photoreduction of CO<sub>2</sub> to hydrocarbon fuels via magnesiothermally reduced TiO<sub>2</sub> photocatalyst. *Applied Catalysis B: Environmental*, 215: 28–35. <https://doi.org/10.1016/j.apcatb.2017.05.028>

**Rehman, S., Ullah, R., Butt, A. M., Gohar, N. D. 2009.** Strategies of making TiO<sub>2</sub> and ZnO visible light active. *Journal of Hazardous Materials*, 170(2–3): 560–569. <https://doi.org/10.1016/j.jhazmat.2009.05.064>

**Ritala, M., Leskela, M. 2002.** Chapter 2: Atomic Layer Deposition (Vol. 1).

**Rossnagel, S. M. 2003.** Thin film deposition with physical vapor deposition and related technologies. *Journal of Vacuum Science & Technology A: Vacuum, Surfaces, and Films*, 21(5): S74–S87. <https://doi.org/10.1116/1.1600450>

**Rueda-Marquez, J. J., Levchuk, I., Fernández Ibañez, P., Sillanpää, M. 2020.** A critical review on application of photocatalysis for toxicity reduction of real wastewaters. *Journal of Cleaner Production*, 258: 120694. <https://doi.org/10.1016/j.jclepro.2020.120694>

**Samsudin, E. M., Goh, S. N., Wu, T. Y., Ling, T. T., Hamid, S. B. A., Juan, J. C. 2015.** Evaluation on the photocatalytic degradation activity of reactive Blue 4 using pure anatase nano-TiO<sub>2</sub>. *Sains Malaysiana*, 44(7): 1011–1019. <https://doi.org/10.17576/jsm-2015-4407-13>

**Sartoretti, C. J., Ulmann, M., Alexander, B. D., Augustynski, J., Weidenkaff, A. 2003.** Photoelectrochemical oxidation of water at transparent ferric oxide film electrodes. *Chemical Physics Letters*, 376(1–2): 194–200. [https://doi.org/10.1016/S0009-2614\(03\)00910-2](https://doi.org/10.1016/S0009-2614(03)00910-2)

**Schwarzenbach, R. P., Egli, T., Hofstetter, T. B., von Gunten, U., Wehrli, B. 2010.** Global Water Pollution and Human Health. *Annual Review of Environment and Resources*, 35(1): 109–136. <https://doi.org/10.1146/annurev-environ-100809-125342>

**Serpone, N., Emeline, A. V., Horikoshi, S., Kuznetsov, V. N., Ryabchuk, V. K. 2012.** On the genesis of heterogeneous photocatalysis: A brief historical perspective in the period 1910 to the mid-1980s. *Photochemical and Photobiological Sciences*, 11(7): 1121–1150. <https://doi.org/10.1039/c2pp25026h>

**Shah, D., Patel, D. I., Roychowdhury, T., Rayner, G. B., O'Toole, N., Baer, D. R., Linford, M. R. 2018.** Tutorial on interpreting x-ray photoelectron spectroscopy survey spectra: Questions and answers on spectra from the atomic layer deposition of Al<sub>2</sub>O<sub>3</sub> on silicon. *Journal of Vacuum Science & Technology B*, 36(6): 062902. <https://doi.org/10.1116/1.5043297>

**Shi, Y. J., Zhang, R. J., Zheng, H., Li, D. H., Wei, W., Chen, X., Sun, Y., Wei, Y. F., Lu, H. L., Dai, N., Chen, L. Y. 2017.** Optical Constants and Band Gap Evolution with Phase Transition in Sub-20-nm-Thick TiO<sub>2</sub> Films Prepared by ALD. *Nanoscale Research Letters*, 12(1): 1-9 <https://doi.org/10.1186/s11671-017-2011-2>

**Shkir, M., Ganesh, V., Yahia, I. S., AlFaify, S. 2018.** Microwave-synthesis of La<sup>3+</sup> doped PbI<sub>2</sub> nanosheets (NSs) and their characterizations for optoelectronic applications. *Journal of Materials Science: Materials in Electronics*, 29(18): 15838–15846. <https://doi.org/10.1007/s10854-018-9670-3>

**Singh, R., Dutta, S. 2018.** Review article A review on H<sub>2</sub> production through photocatalytic reactions using TiO<sub>2</sub> / TiO<sub>2</sub> -assisted catalysts. *Fuel*, 220: 607–620. <https://doi.org/10.1016/j.fuel.2018.02.068>

**Suda, Y., Kawasaki, H., Ueda, T., Ohshima, T. 2005.** Preparation of nitrogen-doped titanium oxide thin film using a PLD method as parameters of target material and nitrogen concentration ratio in nitrogen/oxygen gas mixture. *Thin Solid Films*, 475: 337–341. <https://doi.org/10.1016/j.tsf.2004.07.047>

**Takeda, S., Suzuki, S., Odaka, H., Hosono, H. 2001.** Photocatalytic TiO<sub>2</sub> thin film deposited onto glass by DC magnetron sputtering. *Thin Solid Films*, 392(2): 338–344. [https://doi.org/10.1016/S0040-6090\(01\)01054-9](https://doi.org/10.1016/S0040-6090(01)01054-9)

**Tehrani-Bagha, A. R., Mahmoodi, N. M., Menger, F. M. 2010.** Degradation of a persistent organic dye from colored textile wastewater by ozonation. *Desalination*, 260(1–3): 34–38. <https://doi.org/10.1016/j.desal.2010.05.004>

**Tian, J. L., Zhang, H. Y., Wang, G. G., Wang, X. Z., Sun, R., Jin, L., Han, J. C. 2015.** Influence of film thickness and annealing temperature on the structural and optical properties of ZnO thin films on Si (1 0 0) substrates grown by atomic layer deposition. *Superlattices and Microstructures*, 83: 719–729. <https://doi.org/10.1016/j.spmi.2015.03.062>

**Van Bui, H., Grillo, F., Van Ommen, J. R. 2017.** Atomic and molecular layer deposition: off the beaten track. *Chemical Communications*, 53(1): 45–71. <https://doi.org/10.1039/c6cc05568k>

**Viezbicke, B. D., Patel, S., Davis, B. E., Birnie, D. P. 2015.** Evaluation of the Tauc method for optical absorption edge determination: ZnO thin films as a model system. *Physica Status Solidi (B) Basic Research*, 252(8): 1700–1710. <https://doi.org/10.1002/pssb.201552007>

**Vu, N., Kaliaguine, S., Do, T. 2019.** Critical aspects and recent advances in structural engineering of photocatalysts for sunlight-driven photocatalytic reduction of CO<sub>2</sub> into fuels. *Advanced Functional Materials*, 29(31): 1–44. <https://doi.org/10.1002/adfm.201901825>

**Wang, Jinfeng, Zhao, J., Sun, lu, Wang, X. 2015.** A review on the application of photocatalytic materials on textiles. *Textile Research Journal*, 85(10): 1104–1118. <https://doi.org/10.1177/0040517514559583>

**Wang, Junpeng, Wang, Z., Huang, B., Ma, Y., Liu, Y., Qin, X., Zhang, X., Dai, Y. 2012.** Oxygen vacancy induced band-gap narrowing and enhanced visible light photocatalytic activity of ZnO. *ACS Applied Materials and Interfaces*, 4(8): 4024–4030. <https://doi.org/10.1021/am300835p>

**Wang, Rang, Hashimoto, K., Fujishima, A., Chikuni, M., Kojima, E., Kitamura, A., Shimohigoshi, M., Watanabe, T. 1998.** Photogeneration of highly amphiphilic TiO<sub>2</sub> surfaces. *Advanced Materials*, 10(2): 135–138.

**Wang, Rong, Hashimoto, K., Fujishima, A., Chikuni, M., Kojima, E., Kitamura, A., Shimohigoshi, M., Watanabe, T. 1997.** Light-induced amphiphilic surfaces [4]. *Nature*, 388(6641): 431–432. <https://doi.org/10.1038/41233>

**Wang, Y. H., Ma, Q., Zheng, L. L., Liu, W. J., Ding, S. J., Lu, H. L., Zhang, D. W. 2016.** Performance improvement of atomic layer-deposited ZnO/Al<sub>2</sub>O<sub>3</sub> thin-film transistors by low-temperature annealing in air. *IEEE Transactions on Electron Devices*, 63(5): 1893–1898. <https://doi.org/10.1109/TED.2016.2540679>

**Wolfrum, E. J., Huang, J., Blake, D. M., Maness, P. C., Huang, Z., Fiest, J., Jacoby, W. A. 2002.** Photocatalytic oxidation of bacteria, bacterial and fungal spores, and model biofilm components to carbon dioxide on titanium dioxide-coated surfaces. *Environmental Science and Technology*, 36(15): 3412–3419. <https://doi.org/10.1021/es011423j>

**Wong, M., Chu, W., Sun, D., Huang, H., Chen, J., Tsai, P., Lin, N., Yu, M., Hsu, S., Wang, S., Chang, H., Icrobiol, A. P. P. L. E. N. M. 2006.** Visible-Light-Induced Bactericidal Activity of a Nitrogen-Doped Titanium Photocatalyst against Human Pathogens. *72(9)*: 6111–6116. <https://doi.org/10.1128/AEM.02580-05>

**Xie, Q., Jiang, Y. L., Detavernier, C., Deduytsche, D., Van Meirhaeghe, R. L., Ru, G. P., Li, B. Z., Qu, X. P. 2007.** Atomic layer deposition of Ti O<sub>2</sub> from tetrakis-dimethyl-amido titanium or Ti isopropoxide precursors and H<sub>2</sub> O. *Journal of Applied Physics*, *102(8)*: 0–6. <https://doi.org/10.1063/1.2798384>

**Yadav, H. M., Kim, J. S., Pawar, S. H. 2016.** Developments in photocatalytic antibacterial activity of nano TiO<sub>2</sub>: A review. *Korean Journal of Chemical Engineering*, *33(7)*: 1989–1998. <https://doi.org/10.1007/s11814-016-0118-2>

**Yaseen, D. A., Scholz, M. 2019.** Textile dye wastewater characteristics and constituents of synthetic effluents: a critical review. *International journal of environmental science and technology*, *16(2)*, 1193-1226.

**Yeap, K. L., Teng, T. T., Poh, B. T., Morad, N., Lee, K. E. 2014.** Preparation and characterization of coagulation/flocculation behavior of a novel inorganic-organic hybrid polymer for reactive and disperse dyes removal. *Chemical Engineering Journal*, *243*: 305–314. <https://doi.org/10.1016/j.cej.2014.01.004>

**Yen, C. Y., Jian, S. R., Chen, G. J., Lin, C. M., Lee, H. Y., Ke, W. C., Liao, Y. Y., Yang, P. F., Wang, C. T., Lai, Y. S., Jang, J. S. C., Juang, J. Y. 2011.** Influence of annealing temperature on the structural, optical and mechanical properties of ALD-derived ZnO thin films. *Applied Surface Science*, *257(17)*: 7900–7905. <https://doi.org/10.1016/j.apsusc.2011.04.088>

**Yu, J., Zhao, X., Zhao, Q. 2001.** Photocatalytic activity of nanometer TiO<sub>2</sub> thin films prepared by the sol-gel method. *Materials Chemistry and Physics*, *69(1–3)*: 25–29. [https://doi.org/10.1016/S0254-0584\(00\)00291-1](https://doi.org/10.1016/S0254-0584(00)00291-1)

**Zandi, O., Klahr, B. M., Hamann, T. W. 2013.** Highly photoactive Ti-doped  $\alpha$ -Fe<sub>2</sub>O<sub>3</sub> thin film electrodes: Resurrection of the dead layer. *Energy and Environmental Science*, *6(2)*: 634–642. <https://doi.org/10.1039/c2ee23620f>

**Zhang, J., Tian, B., Wang, L., Xing, M., & Lei, J. (2018).** Mechanism of Photocatalysis. *Photocatalysis: fundamentals, materials and applications*, Springer, Singapore, 1–15 pp. [https://doi.org/10.1007/978-981-13-2113-9\\_1](https://doi.org/10.1007/978-981-13-2113-9_1)

**Zhang, L., Fang, M. 2010.** Nanomaterials in pollution trace detection and environmental improvement. *Nano Today*, *5(2)*: 128–142. <https://doi.org/10.1016/j.nantod.2010.03.002>

**Zulfiqar, Yuan, Y., Yang, J., Wang, W., Ye, Z., Lu, J. 2016.** Structural and optical properties of (Zn, Co) co-doped SnO<sub>2</sub> nano particles. *Journal of Materials Science*:

Materials in Electronics, 27(11): 12119–12127.

## RESUME

Name Surname : Shafiqul Islam  
Place and Date of Birth : Chittagong/01.01.1994  
Foreign Languages : Turkish, English, Hindi, Urdu

Education Status  
High School : Govt. Hazi Muhammad Mohsin College, Bangladesh  
Bachelor's : University of Chittagong, Textile Engineering, Bangladesh  
Master's : Bursa Uludag University, Textile Engineering, Turkey

Work Experience : Graduate Research Assistant  
(TÜBİTAK Scientific Project)

Contact (e-mail) : shafiqislam94@gmail.com

Paper : **Islam, S., Akyıldız, H. A. 2020.** Photocatalytic Activities of ALD TiO<sub>2</sub>, ZnO and Al<sub>2</sub>O<sub>3</sub> film On Glass Fabrics. 6th International Fiber and Polymer Research Symposium, 24-25 January 2020, BUU, Bursa.